Heliyon 10 (2024) e36227

Contents lists available at ScienceDirect

Heliyon

journal homepage: www.cell.com/heliyon

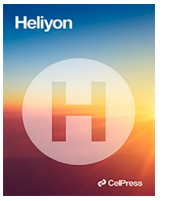

Research article

Alkaline saline lakes: A chemical evolution experiment evaluating the stability of formaldehyde in an aqueous saline environment

Claudio Alejandro Fuentes-Carreón [a,b,*], Adriana Leticia Meléndez-López [a,c], Jorge Armando Cruz-Castañeda [a], Alicia Negrón-Mendoza [a,**]

[a] Instituto de Ciencias Nucleares, Universidad Nacional Autónoma de México, Cd. Universitaria, México City, Mexico
[b] Universidad Nacional Autónoma de México, Cd. Universitaria, México City, Mexico
[c] Escuela Nacional de Ciencias de la Tierra, Universidad Nacional Autónoma de México, Cd. Universitaria, México City, Mexico

ARTICLE INFO

Keywords:
Prebiotic chemistry
Aldehydes
Clay minerals
Chemical evolution

ABSTRACT

Formaldehyde condensation in the presence of a mineral catalyst and under alkaline conditions is considered to be a "messy" chemical system due to its dependence on the complex chemical equilibrium between the reaction intermediates, which has a significant impact on the final products.

This chemical system is extremely important in prebiotic chemistry and has been proposed as a potential pathway for carbohydrate formation in the early Earth. Saline and soda lakes are alkaline systems that could concentrate and accumulate a wide variety of ions (such as phosphate) and clay minerals, which can catalyze prebiotic chemical reactions. These geological environments have recently been suggested as ideal environments in which prebiotic chemical reactions could have occurred.

This study uses Lake Alchichica in Mexico as a physicochemical analog of an early Archean saline lake to examine the stability of formaldehyde in these aqueous saline environments. Formaldehyde decomposes into sugar-like and CHO molecules in alkaline, high-salinity environments depending on the minerals phases present. As phosphate ion (HPO_4^{2-}) is available in the aqueous medium, the results of our experiments also imply that phosphorylation processes may have occurred in these natural settings.

1. Introduction

The term “chemical evolution” refers to the suite of hypotheses that attempt to explain how the first components of life (*i.e.*, biomolecules) were abiotically generated from multiple organic compounds. This idea, proposed independently by Oparin and Haldane in the 1920s [1], was verified experimentally using the spark discharge experiment designed by S. Miller [2]. Following this, several prebiotic chemical pathways have been proposed in an attempt to explain the formation of the aforementioned biomolecule precursors.

Chemical evolution experiments (*i.e.*, prebiotic chemistry studies) involve the simulation of primitive Earth environments, such as the primeval ocean and ancient hydrothermal systems. Many of these environments share some common characteristics, such as the

* Corresponding author. Instituto de Ciencias Nucleares, Universidad Nacional Autónoma de México, Cd. Universitaria, México City, Mexico.
** Corresponding author.
E-mail addresses: claudio.fuentes@ciencias.unam.mx (C.A. Fuentes-Carreón), negron@nucleares.unam.mx (A. Negrón-Mendoza).

https://doi.org/10.1016/j.heliyon.2024.e36227
Received 4 June 2024; Received in revised form 9 August 2024; Accepted 12 August 2024
Available online 13 August 2024

presence of an aqueous medium and a mineral phase. These factors play an important role in prebiotic chemical reactions, either as catalysts or as initiators of organic synthesis [3]. One clear example is the formose reaction [4], which involves the condensation of formaldehyde into aldehydes and carbohydrates under basic conditions [5]. This reaction requires alkaline conditions, heat, and the presence of carbonate minerals, which function as inorganic catalysts. These carbonate minerals can also influence the stability of the formed sugars, allowing for the formation of complex compounds [6]. Additionally, the active surfaces of some mineral phases, such as clays or iron hydroxide minerals, can further promote these aldehyde condensation reactions [7]. However, it should be noted that specific sugars, such as ribose or glucose, are merely by-products of these reactions; the main condensation products of these reactions comprise a complex mixture of straight-chain and cyclic pentoses and hexoses [8]. Therefore, studies on the reaction mechanisms of these prebiotic reactions in simulated early Earth environments are of great importance, as they are necessary to correctly describe how the building blocks of life could have emerged on the early Earth.

Aldehydes are of particular interest in the field of chemical evolution as they play a wide variety of roles in abiotic synthesis reactions. Formaldehyde can yield sugars when heated under alkaline conditions in the presence of a mineral catalyst [8]. Acetaldehyde has been proposed as a source of alanine [9], while multiple intermediaries of the formose reaction, such as pyruvaldehyde, glyceraldehyde, and glyoxal, have been shown to play an important role in carbohydrate formation. Besides their ability to form sugars, the phosphorylation of aldehydes is of particular interest, as several phosphate compounds, such as glyceraldehyde 3-phosphate, are essential metabolites in multiple metabolic pathways [10]. Consequently, the study of how these compounds could have formed in prebiotic environments has become a central topic in modern chemical evolution studies.

As previously mentioned, solid surfaces may have played an important role in the chemical evolution of minerals by serving as catalysts in the synthesis of organic compounds [3]. Of the mineral surfaces readily available on the early Earth, clay minerals have been highlighted as a crucial component for surface chemical processes. These minerals can selectively concentrate specific organic molecules. Also, the adsorption of organic molecules onto mineral surfaces can protect them from degradation by ionizing radiation [11]. Mineral surfaces can also catalyze the polymerization of organic molecules [12]. Clays have been ubiquitous mineral phases ever since their formation during planetary accretion [13]. Consequently, clays could have played an important role in the prebiotic synthesis of organic compounds due to their abundance on the early Earth.

However, phosphorylation reactions highlight the difficulties with prebiotic chemical reactions in aqueous mediums, where the formation of the final product is not thermodynamically favored. As phosphorylation is a dehydration reaction (*i.e.*, releases water), this process could not have occurred readily in an aqueous medium, as any reaction products would rapidly hydrolyze. Furthermore, dissolved phosphate is relatively rare in natural environments [14]. Consequently, phosphate is not expected to have existed in high concentrations on the early Earth because its concentration is buffered by the dissolution of phosphate minerals [15].

In light of this "phosphate problem", alternative mechanisms have been proposed for the phosphorylation reactions and the occurrence of phosphate concentrations in natural environments. One novel idea proposes that carbonate-rich saline lakes could have been a natural environment in which up to 1 mol L^{-1} of phosphate could have accumulated [16]. Specifically, the precipitation of phosphate with calcium to form low-solubility apatite minerals would have been inhibited by the sequestration of Ca^{2+} into carbonate minerals, increasing the availability of dissolved phosphate in the medium. Therefore, carbonate-rich saline lakes could have been an important geological environment in which sugar-forming prebiotic reactions could have occurred, especially due to their favorable physicochemical characteristics, such as their high pH values (>9) as well as the abundance of dissolved metallic cations (Ca^{2+}, Na^{+}, Mg^{2+}, etc.), which have been shown to catalyze formose-like reaction of aldehydes [5,6,8]. As clays are a common mineral phase that are present in lacustrine sediments [17]; these minerals could have further catalyzed sugar-forming reactions.

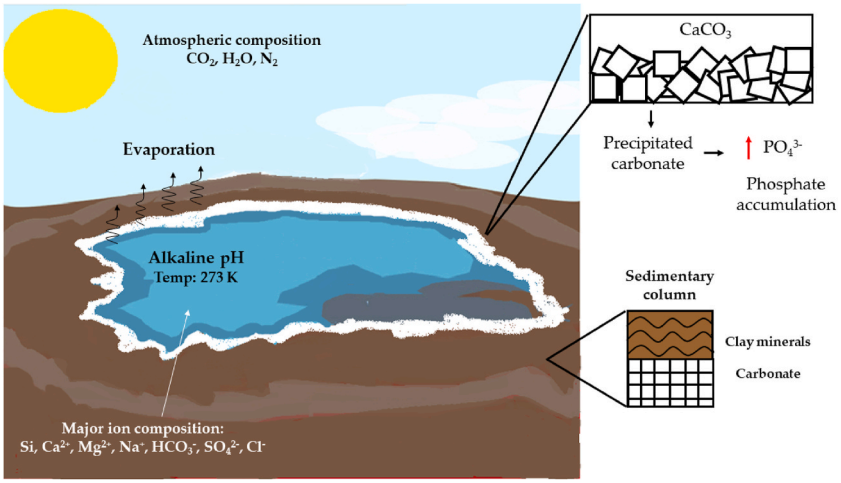

Fig. 1. Schematic representation of an ancient saline lake. The atmospheric composition denoted in the illustration follows the model proposed by Ref. [23]. These aqueous environments may have been abundant during the Archean (~3.9 Ga) in crustal zones with a high incidence of tectonic activity, which would have resulted in the formation of basins in which saline water could have accumulated.

1.1. Lake Alchichica as an analog of an ancient saline carbonate-rich lake

Lake Alchichica is a crater lake located in the Cuenca de Oriental in central Mexico. The crater is a maar formed by a phreato-magmatic eruption and is surrounded by tuff deposits [18]. Alchichica is a closed basin lake, with no surface water tributaries or outlets. The water balance is maintained by precipitation and evaporation. The major ions present in the lake waters include Na^+, Cl^-, Mg^{2+}, and SO_4^{2-}, with K^+, Ca^{2+}, Li^+, Br^-, and F^- existing as minor constituents. The hardness of the lake waters has been measured to be 18.72 mmol L^{-1}, which indicates that the lacustrine system is naturally saturated in $CaCO_3$ [19]. Phosphate can be found in concentrations of up to 5.16 μmol L^{-1} [20]. A few studies have been conducted on the mineralogical composition of the lake sediments [21]. reports that the sediment comprises mainly carbonate minerals and silt deposits (predominantly clays). The geochemical characteristics of this crater lake make it an ideal analog for ancient saline lakes (Fig. 1). These ancient aqueous surface environments could have been formed due to the chemical weathering of volcanic rocks in a CO_2-rich atmosphere [16]. The high amounts of volcanic and tectonic activity could have formed lake basins due to the continuous generation of young crust [22], which, in turn, would be filled by the surface water enriched in weathering products. As Lake Alchichica is a saline lake rich in calcium carbonates, this environment is an ideal candidate for the accumulation of phosphate in accordance with previously proposed models [16]. Furthermore, the alkaline pH of the lake waters as well as its ionic content represent chemical characteristics that would have been ideal for the base-catalyzed aldolic condensation reactions of aldehydes and ketones dissolved in the medium. This work aims to study the stability of formaldehyde and its decomposition products in an aqueous saline environment that is analogous to an ancient saline lake; it will also focus on the presence of clay minerals in these environments and how they could have influenced the stability of the aldehyde in the system.

2. Materials and methods

2.1. Reagents

DL-glyceraldehyde (90 %) paraformaldehyde (99.9 %), glyoxal (40 wt % in H_2O), glycolaldehyde (>90 %), D-glucose (99.9 %), D-ribose (99.9 %), Sucrose (99.9 %), NaOH (99 %), HCl (37 wt % in H_2O), D_2O (99.8 %), NaCl, $MgSO_4 \bullet 7H_2O$, and $Na_2HPO_4 \bullet 7H_2O$ were obtained from Sigma-Aldrich®, St. Louis, MO, USA. Methanol-free formaldehyde was prepared from paraformaldehyde according to the method described by Ref. [24]. Acetonitrile (HPLC), ethanol (HPLC), H_2SO_4 (95–97 %), α-D-Glucose 1-phosphate disodium salt hydrate (97 %), and 2,4-dinitrophenylhydrazine (DNPH) (97 %) were obtained from Merck Co.®, Kenilworth, NJ, USA. Ca-Montmorillonite (STx-1; Gonzales County, Texas, USA) and Na-Montmorillonite (SWy-2; Crook County, Wyoming, USA) were obtained from the Source Clay Minerals Repository, Purdue University, IN, USA. All the reagents were of the highest available commercial purity.

2.2. Preparation of samples

To simulate the physicochemical conditions of Lake Alchichica, saline water with an ionic content analogous to the Alchichica system was prepared. This analog consisted of an aqueous solution of 0.02 mol L^{-1} NaCl, 1×10^{-3} mol L^{-1} $MgSO_4 \bullet 7H_2O$, and 0.05 mol L^{-1} $Na_2HPO_4 \bullet 7H_2O$. These salt concentrations were used to simulate the major ions present in the waters of Lake Alchichica [20], in which the total water column concentration of Na^+, Cl^-, Mg^{2+}, and SO_4^{2-} were reported to be approximately 100, 87, 35, and 16 meq L^{-1}, respectively [20]. An exception was made with $MgSO_4 \bullet 7H_2O$, whose concentration was increased to increase the solubility of the salt at the desired volumes (100 mL). The total ion content, pH, ionic force, and temperature of the saline water samples are presented in Table 1. This water was used for the preparation of concentrated (1.5 mol L^{-1}) aqueous methanol-free formaldehyde solutions. The samples were degasified with Ar to remove any dissolved O_2. The final pH of the formaldehyde standard solution in saline water was 9.13.

2.3. Sorption experiments

100 mg of clay mineral phases were mixed with 5 mL aliquots of the degasified formaldehyde standard solution dissolved in saline water in 15-mL polyallomer centrifuge tubes (Beckman Coulter®, Brea, CA, USA) to simulate the interaction between formaldehyde and clays in a saline, alkaline environment. Two different sets of clay suspensions inside polyallomer tubes were done, using different clays in each one (Na-Montmorillonite (SWy-2) and Ca-Montmorillonite (STx-1)) The polyallomer tubes with clay suspension were

Table 1
Physicochemical characteristics of simulated Lake Alchichica saline water.

Ion	Concentration (mol L^{-1})	Temperature (K)	System pH	Ionic Force (I)
Na^+	0.12	298	9.2	0.173
Cl^-	0.02			
Mg^{2+}	1×10^{-3}			
SO_4^{2-}	1×10^{-3}			
HPO_4^{2-}	0.05			

saturated with Ar to create an anoxic atmosphere and the polyallomer tubes were sealed to preserve the atmospheric integrity of the system.

Once prepared in the polyallomer tubes, the clay-formaldehyde mixtures were subjected to constant agitation. The minerals were separated from the aqueous phase using an Allegra XL-90 centrifuge (Beckman Coulter®, Brea, CA, USA) at 25,000 rpm at room temperature for 15 min at defined time intervals (1, 24, 48, 168, and 336 h). The mineral powder was desiccated and preserved for further analysis. The collected supernatants were filtered using 12-μm Acrodisc syringe filters (Whatman®, Chicago, IL, USA) and stored at 0 °C for the subsequent High pressure liquid chromatography (HPLC) measurements. The formation of new organic compounds in the sample supernatants was monitored by HPLC; analyzing each sample after the previously described sorption time intervals elapsed. Following this analysis, the aqueous phase was evaporated under a constant air flow until the dissolved organic compounds precipitated. The precipitate—a white powder—was stored in a vacuum desiccator for 24 h to remove excess water in the samples and stored for further analysis.

2.4. Carbonyl-containing compound measurements

The aldehydes were identified in the form of their 2,4-dinitrophenylhydrazine (DNPH) derivatives using HPLC–UV. The carbonyl compounds were derivatized by reacting 4 mL aliquots of the sample supernatants with 4 mL aliquots of the DNPH reagent (0.4 mg DNPH dissolved in 2 mL H_2SO_4, 3 mL H_2O, and 25 mL of ethanol) for 12 h. The carbonyl derivatives precipitated as yellow-orange crystals, which were filtered, dried, recrystallized, and redissolved in acetonitrile for subsequent analysis. The DNPH derivatives of formaldehyde, glyoxal, pyruvaldehyde, and DL-glyceraldehyde were prepared and used as standards for the detection of carbonyl compounds in the experimental samples.

2.5. Sample analysis: sorption experiments

2.5.1. Raman spectroscopy analysis

Raman spectroscopy was used to identify the chemical structure of the organic standards and the reaction products. The organic solids precipitated from the experimental samples were pressed between a NaCl pellet and their Raman spectra were collected using an Optosky ATR 3000 portable Raman spectrometer. The Raman probe, which utilized a Class IIIB laser, was positioned at an operating distance of 6 mm from the sample. The laser was maintained at a constant power of 400 mW to avoid damage to the sample. The spectra were recorded in the interval of 3000 to 150 cm^{-1} with a resolution of ± 5 cm^{-1}.

2.5.2. IR-ATR spectroscopy

The infrared spectra of the precipitated organic solids (a dry organic powder) as well as the clays before and after sorption (as a dry mineral powder) were collected using attenuated total reflectance–Fourier transform infrared (ATR-FTIR) spectroscopy. Spectra was collected with a PerkinElmer® Spectrum 100-FTIR-ATR spectrometer, coupled to a Horizontal Attenuated Total Reflectance (HATR) accessory with a reflection element consisting of a ZnSe crystal (PerkinElmer®). The angle of incidence into the crystal cell was 45°. Prior to each batch sample, a background spectrum of the environment and empty cell was collected. The spectra were recorded in the interval of 4000 to 650 cm^{-1} with a resolution of 4 cm^{-1} using 25 scans per sample.

2.5.3. Analysis of remnant phosphate after sorption with STx-1 and SWy-2 clays

The remnant ion phosphate (HPO_4^{2-}) in solution was determined by conducting an acid-base titration of the aqueous supernatant of the samples after sorption with STx-1 and SWy-2 clays. 0.01 mol L^{-1} NaOH was used as a titrant, which allowed us to quantify the formation of Na_2HPO_4 in the system, which possessed an equivalence point of pH 9.4. The full description of the method used can be found in Ref. [25]. The pH of the sample supernatants after sorption was 7.8 and 8.12 for the STx-1 and SWy-2 samples, respectively. Consequently, all samples were acidified with 0.1 mol L^{-1} HCl to a pH of 6.0. NaOH was subsequently added to 5 mL aliquots of the supernatants, with pH constantly monitored until the equivalence point was reached. The concentration of phosphate at the equivalence point was calculated based on the total titrant volume. This procedure was also conducted on the original saline solutions to determine the phosphate concentration in the system before sorption. The tritation curve of the experimental samples was monitored using a ThermoScientific® VersaStar Pro pH meter coupled to an Orion ROSS 8157 UWMMD pH/ATC triode electrode.

2.5.4. HPLC analysis

A Waters® ACQUITY UPLC evaporative light scattering (ELS) detector coupled to a Waters® 600E multisolvent delivery system was used to characterize the sugars and CHO compounds present in the samples using their retention times. The compounds were separated in a GL Sciences® Inerstil NH_2 5 μm column (4.6 × 250 mm; Torrance, CA, USA) using isocratic elution at 1.0 mL/min with a mobile phase comprising 60 % acetonitrile and 40 % water.

An HPLC coupled to an electrospray ionization-mass spectroscopy (ESI-MS) detector was used to analyze the *m/z* of the detected sugar-like compounds. This analysis was conducted using a Waters® 515 HPLC pump coupled to a Waters® SQ-2 Single Quadrupole Mass Detector system, with electrospray ionization in negative (ESI-) mode. The cone voltage was 20 V, the capillary voltage was 2.55 kV, and the desolvation temperature was 350 °C. The sugar-like compounds were separated using the aforementioned GL Sciences® Inerstil NH_2 5 μm column (4.6 × 250 mm) using isocratic elution at 0.8 mL/min with a mobile phase comprising of 60 % acetonitrile and 40 % water; this method was specifically designed for the separation of carbohydrates.

A Knauer®, Berlin, Germany Azura P 4.1s HPLC pump equipped with a Knauer® Smartline 2300 refraction index (RI) detector was

used to analyze the phosphorylated compounds. The stationary phase was an Alltech® Wescan 10 μm Anion Exclusion column (7.5 × 300 mm; Illinois, USA); the procedure utilized isocratic elution at 0.5 mL/min with a mobile phase of 1.5 mmol L^{-1} H_2SO_4 in 10 % acetonitrile. All chromatographic measurements were done at 588 mm Hg pressure and 25 °C.

2.5.5. ^{31}P Nuclear magnetic resonance (^{31}P NMR)

^{31}P NMR spectra of the precipitated organic solids formed after sorption with SWy-2, and STx-1 clays was recorded using a Bruker®, Fällanden, Switzerland 400 MHz Avance III HD spectrometer. 5 mg of the precipitated organic solids were dissolved in 0.7 mL of D_2O, and then transferred to 5 mm tubes to collect the ^{31}P NMR spectra. The NMR measurements were done at 588 mm Hg and 25 °C.

2.6. Sample analysis: carbonyl-containing compounds

2.6.1. HPLC-UV

HPLC-UV was used to analyze the DNPH derivatives of the carbonyl-containing compounds. A Varian® 9010 Solvent Delivery System HPLC pump (California, USA) coupled to a Varian® 9060 Variable Wavelength UV–Vis detector was used. The derivatives of the carbonyl compounds were monitored by measuring their absorbance at 350 nm. The derivatives were separated in a SUPELCO® Supelcosil LC-18 C-18 column (250 × 4.6 mm) using isocratic elution at 1.0 mL/min with a mobile phase comprising 70 % acetonitrile and 30 % water. The results were collected using an HP® 3396A Integrator (California, USA).

2.7. Analysis of chemical equilibria in the aqueous solution

Following the equilibration of salts in the system, the total ionic concentration and saturation index (SI) of all possible solids in solution were modeled using the Chemical Equilibrium Modeling System MINEQL + Version 5.0 computer program, which has been distributed as free software.

MINEQL+ is designed for the modelling of chemical equilibria and uses a numerical engine to solve mass balance equations using equilibrium constants. The theoretical considerations and equations that underpin the MINEQL engine are discussed in detail in Ref. [26]. The equilibrium constant values were referenced from the USEPA MINTEQA2 thermodynamic database [27]. The following values were used for the initial concentration of ionic species in solution: 0.12 mol L^{-1} Na^+, 0.02 mol L^{-1} Cl^+, 1×10^{-3} mol L^{-1} Mg^{2+}, and 1×10^{-3} mol L^{-1} SO_4^{2-}. Phosphate was introduced into the system in the form of the HPO_4^{2-} ion (0.05 mol L^{-1}). All equilibrium equations were solved using a pH of 9.13, an ionic force (I) of 0.174 (calculated using the Debye-Hückel Davies equation [28]), a temperature of 288 K, and a pCO_2 of 3.5 atm. The temperature and pCO_2 values were selected based on the environmental conditions used for the sorption experiments. The theoretical calculations were repeated using a pCO_2 of 0.3 bar and a temperature of 288 K to simulate the equilibria expected under early Archean environmental conditions [29].

3. Results

3.1. Formaldehyde and clay analysis

The IR pattern of both Na-montmorillonite (SWy-2; Fig. 2) and Ca-montmorillonite (STx-1; Fig. 3) exhibit vibrational bands associated with Si–O bonds at 797 and 697 cm^{-1} for SWy-2 and 797 and 693 cm^{-1} for STx-1. Vibrational bands associated with OH groups were present in both clays (Figs. 2a and 3a). Based on the literature, the 883 cm^{-1} and 863 cm^{-1} bands in SWy-2 (Fig. 2b) were attributed to the vibration of $AlFe^{3+}OH$ and AlMgOH, respectively [30], while the 843 cm^{-1} band in STx-1 (Fig. 3b) was interpreted to be due to the vibration of MgOH groups.

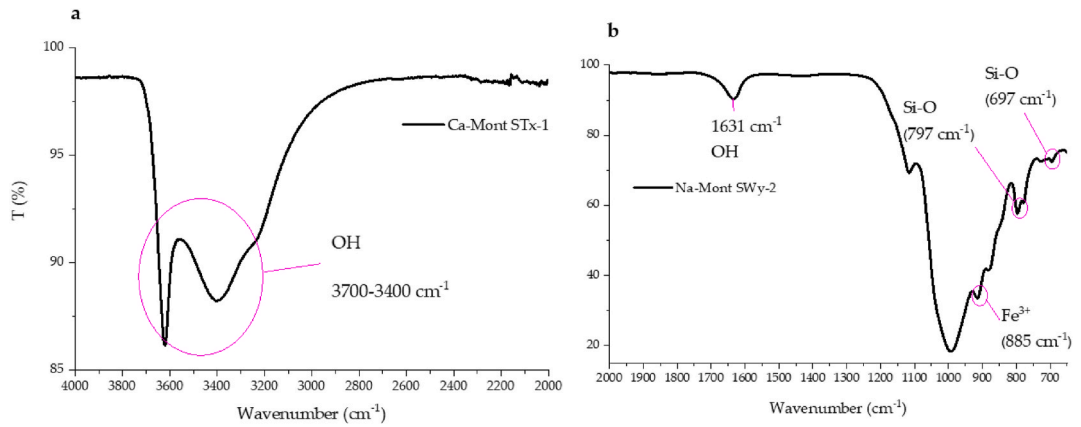

Fig. 2. IR spectrum of the natural Na-montmorillonite (SWy-2) samples. a) 4000–2000 cm^{-1} region. b) 2000–650 cm^{-1} region.

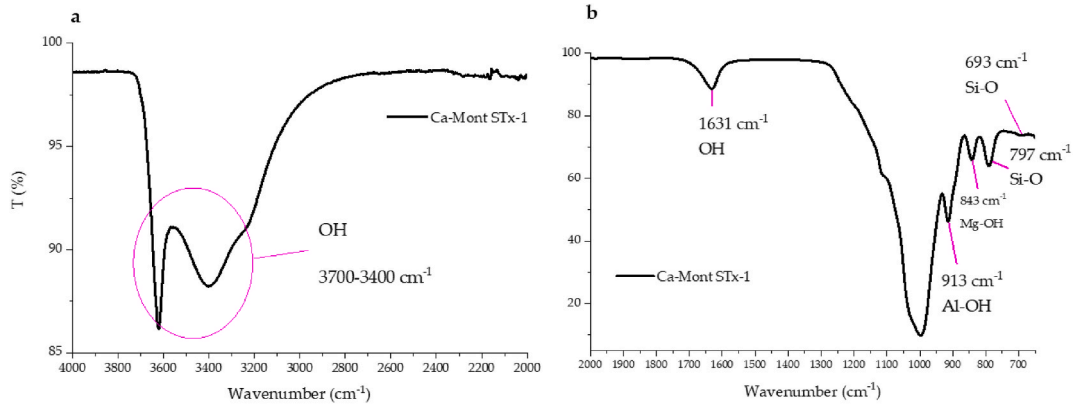

Fig. 3. IR spectrum of the natural Ca-montmorillonite (STx-1) samples. a) 4000–2000 cm^{-1} region. b) 2000–650 cm^{-1} region.

The IR spectrum of paraformaldehyde (the precursor from which the methanol-free formaldehyde was prepared) exhibits vibrational bands associated with sp^3 carbons at 2981, 2921, and 1468 cm^{-1} (Fig. 4). The 1088 cm^{-1} vibration band is associated with the asymmetric C–O stretch. These observations suggest that the sample consists of pure crystalline paraformaldehyde. A weak band around 3000 cm^{-1} was also observed: These vibrations could be associated with OH groups present in the sample. However, the lack of the C–OH stretch vibration band suggests that the main C–O bond on the organic compound is an ether bond.

3.2. *Chemical equilibrium of the simulated Lake Alchichica saline Water*

The stability of formaldehyde in an aqueous saline environment, such as the chemical analog of an ancient saline lake, is influenced by the complex equilibrium in the saline solution. Consequently, it is important to consider the relative concentration of species in such solutions.

We determined the total ion concentration of the dissolved species in the simulated Lake Alchichica saline solution at 25 °C in an O_2-free atmosphere with a pCO_2 of 3.5 atm. The total concentration of non-precipitated ionic species in the saline water solution is presented in Table 2. The amount of free phosphate (PO_4^{3-}) in solution was less than 0.05 mol L^{-1} due to the presence of additional chemical species that removed this ion from the medium. Due to the high Na concentration of the waters (0.12 mol L^{-1}), $NaHPO_4^-$ was one of the major phosphate species present in solution, accounting for up to 26 % of the total P in the system (Table 3). Soluble phosphate in the form of HPO_4^{2-} was present at concentrations of 3.56×10^{-2} mol L^{-1}, representing 71.3 % of the total P. The discrepancy in the concentrations of the phosphate ions in the calculated experimental values can be attributed to dispersion in the pH

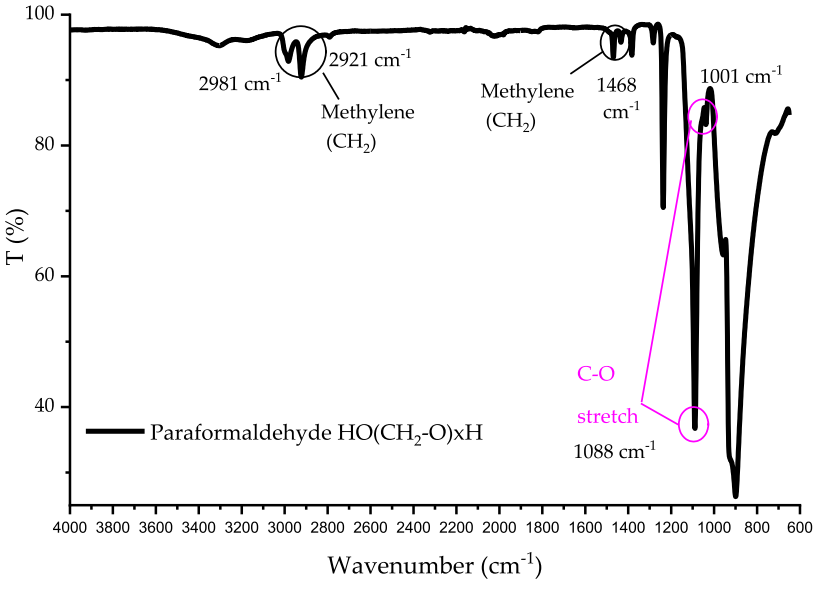

Fig. 4. IR spectrum of paraformaldehyde powder.

Table 2
Total concentration of dissolved ionic species in the simulated Lake Alchichica saline water.

Ion	Concentration (mol L^{-1})
[Na^+]	0.12
[Cl^-]	0.02
[Mg^{2+}]	5.68×10^{-4}
[SO_4^{2-}]	1×10^{-3}
[PO_4^{3-}]	4.97×10^{-2}
[CO_3^{2-}]	1.12×10^{-2}

measurements; specifically, pH electrodes lose precision at high Na^+ concentrations due to the saturation of the exchange membrane. An analysis of the SI of all possible solids in solutions reveals the complex equilibrium of the potential mineral phases. Positive SI values are associated with mineral phases that are likely to precipitate in the system, while negative values are associated with mineral species that are presented but are undersaturated and unlikely to precipitate. At the present temperature, pH, and chemical conditions, we found that the only mineral species in equilibrium with the ion concentration was $Mg_3(PO_4)_2$ (Table 4). It should be noted that an SI of 0 suggests an unstable equilibrium: changes in the concentration of dissolved Mg^{2+} could favor the precipitation of this mineral phase.

To investigate how the chemical equilibrium of the system would change in a CO_2-rich atmosphere, we repeated the previous calculations using a pCO_2 of 0.3 bar and a temperature of 288 K, which are the partial pressures and global average temperatures characteristic of the early Archean [29]. The total concentration of dissolved ions under these conditions is shown in Table 5. The amount of soluble phosphate was found to have increased by almost 30 % compared to the equilibrium concentrations in the system at modern pCO_2 values, increasing the availability of this ion in saline waters (Table 6). The SI analysis also highlighted the rather complex equilibrium between the mineral phases (Table 7). Magnesite was the only mineral species in equilibrium with the system, likely due to the increase in the atmospheric pressure of CO_2 (~1000 times more than CO_2 preindustrial values).

3.3. Stability of formaldehyde in simulated saline aqueous media

The remaining amount of formaldehyde in the experimental samples was determined by measuring the absorbance of formaldehyde–DNPH at 350 nm as a function of the sorption time, using the Beer–Lambert law to calculate the concentration of the compound in solution. The calibration curve was constructed using formaldehyde–DNPH standards with concentrations ranging between 1×10^{-2} to 1×10^{-5} mol L^{-1}. Besides these determinations, HPLC-UV analysis shows that formaldehyde is labile under the experimental conditions. Formaldehyde decomposes in the presence of clays (Fig. 5). The total percentage of remnant formaldehyde was found to decrease proportionally to sorption time. The decomposition rate of the compound was independent of the type of clay present in the system, though there was a slight increase in decomposition time when exposed to SWy-2 clay: at the maximum sorption time, 94.16 % formaldehyde had decomposed when exposed to STx-1 compared to 98.01 % when exposed to SWy-2. An exhaustive analysis of the aqueous supernatants by HPLC-ESI-MS as well as the organic solids precipitated after the evaporation of the organic sample yielded additional chemical information about the formaldehyde decomposition products.

The precipitated organic solids included contributions from decomposition products, remnants of paraformaldehyde, and traces of Na_2HPO_4 salt. The IR spectrum of the precipitated organic solids formed from sorption onto SWy-2 exhibited vibrational bands associated with sp^3 carbons (2894, 2922 and 1474 cm^{-1}) and C–OH stretching (1084 and 1065 cm^{-1}), as well as a vibrational band at 1622 cm^{-1} (Fig. 6). The precipitated organic solids formed from sorption onto STx-1 exhibited vibrational bands associated with sp^3 and sp^2 carbons as well as C–O bonds (Fig. 7); this contrasts with the products identified in SWy-2, in which the region corresponding to C–O bond vibration was attributed to ether groups.

Raman spectra yielded additional information about the functional groups present in the samples derived from sorption onto the STx-1 and SWy-2 clays (Figs. 8 and 9, respectively). The most notable vibrational bands were found at 1090, 1075, 1052, 910, and 865 cm^{-1}, which correspond to C–O and C–H bond vibrations. The vibrational band at 1600 cm^{-1}, which corresponds to sp^2 carbon (C=C), is present in both systems. The samples derived from sorption onto SWy-2 also exhibited a vibrational band at 1700 cm^{-1} associated

Table 3
Chemical species derived from PO_4^{2-} in the simulated Lake Alchichica saline water.

Chemical species	Concentration (mol L^{-1})	Total %
PO_4^{3-}	8.979×10^{-5}	0.18
$MgH_2PO_4^+$	4.252×10^{-7}	0.00085
$MgHPO_4$(aq)	3.535×10^{-4}	0.707
$NaHPO_4^-$	1.342×10^{-2}	26.8
$H_2PO_4^-$	1.708×10^{-4}	0.342
HPO_4^{-2}	3.566×10^{-2}	71.3
H_3PO_4	1.322×10^{-11}	0
$MgPO_4^-$	1.935×10^{-5}	0.0387
$Mg_3(PO_4)_{2\ (s)}$	1.439×10^{-4}	0.576
Total P	0.04971	100

Table 4
Saturation indices of all possible mineral phases in the simulated Lake Alchichica saline water.

Mineral phase	SI
Hydromagnesite ($Mg_5(CO_3)_4(OH)_2•4H_2O$)	−7.956[a]
Artinite ($Mg_2(CO_3)(OH)_2•3H_2O$)	−3.301[a]
$Mg(OH)_2$	−4.821[a]
Periclase (MgO)	−7.611[a]
Brucite ($Mg(OH)_2$)	−2.871[a]
$MgHPO_4•3H_2O$	−0.452[a]
Nesquehonite ($MgCO_3•3H_2O$)	−3.004[a]
Natron ($Na_2CO_3•10H_2O$)	−4.289[a]
Epsomite ($MgSO_4•7H_2O$)	−5.747[a]
Mirabilite ($NaSO_4•10H_2O$)	−4.686[a]
Halite (NaCl)	−4.58[a]
Magnesite ($MgCO_3$)	−0.214[a]
$Mg_3(PO_4)_2$	0
Thenardite ($NaSO_4$)	−6.122[a]

[a] Negative values indicate the solid is undersaturated in the aqueous system and is thus unable to precipitate.

Table 5
Total concentration of dissolved ionic species in the simulated Lake Alchichica saline water under early Archean conditions.

Ion	Concentration (mol L^{-1})
$[Na^+]$	0.12
$[Cl^-]$	0.02
$[Mg^{2+}]$	2.58×10^{-5}
$[SO_4^{2-}]$	1×10^{-3}
$[PO_4^{3-}]$	0.05
$[CO_3^{2-}]$	1.07×10^{-2}

Table 6
Chemical species derived from PO_4^{2-} in the simulated Lake Alchichica saline water under early Archean conditions.

Chemical species	Concentration (mol L^{-1})	Total %
PO_4^{3-}	9.63×10^{-5}	0.19
$MgH_2PO_4^+$	7.08×10^{-10}	0
$MgHPO_4$(aq)	5.77×10^{-7}	0.0011
$NaHPO_4^-$	1.25×10^{-3}	2.5
$H_2PO_4^-$	2.4×10^{-4}	0.491
HPO_4^{-2}	4.8×10^{-2}	96.8
H_3PO_4	1.71×10^{-11}	0
$MgPO_4^-$	2.51×10^{-8}	0
Total P	0.05	100

with carbonyl bonds (C=O). This vibrational band was notably absent in the samples derived from sorption onto STx-1.

Due to the presence of HPO_4^{2-} ion in the saline solution, additional IR and Raman analysis were done, aimed to study the interaction of this ion with the organic compounds present in solution. Specifically, the formation of organophosphates was monitored. Diagnostic peaks of P–O stretching modes typically appear between 800 and 1300 cm^{-1}; both samples exhibited vibrational bands at 1087, 930, and 862 cm^{-1}, which could correspond to P–O stretching modes of organophosphates (Fig. 10) [31]. Therefore, the band at approximately 975 cm^{-1} can be assigned to the antisymmetric C–O–P stretching vibration of phosphorylated organic compounds [32, 33] (Fig. 9).

HPLC-ESI-MS was used to detect sugar-like compounds in the sample supernatants, which were analyzed following sorption onto SWy-2 (Fig. 12) and STx-1 (Figs. 11 and 12). The retention times of standard carbohydrates are shown in Table 8. Both samples were monitored using the Total Ion Count (TIC) mode with negative ionization. The elution times of standard carbohydrates were used as a reference for the identification of detected compounds (Table 2). The TIC chromatogram exhibited two signals at retention times of 9.2 and 16.4 min; neither of these times matched any of the standard carbohydrates. Furthermore, each signal exhibited multiple *m/z* values (Figs. 11 and 12), suggesting the fragmentation of the separated organic compounds.

In addition to these sugar-like compounds, aldehydes were detected by HPLC-UV (Fig. 13a and 13b). The chromatograms of the

Table 7
Saturation indices of all possible mineral phases in the simulated Lake Alchichica saline water under early Archean conditions.

Mineral phase	SI
Hydromagnesite ($Mg_5(CO_3)_4(OH)_2•4H_2O$)	−11.770[a]
Artinite ($Mg_2(CO_3)(OH)_2•3H_2O$)	−6.795[a]
$Mg(OH)_2$	−7.676[a]
Periclase (MgO)	−11.385[a]
Brucite ($Mg(OH)_2$)	−6.419[a]
$MgHPO_4•3H_2O$	−3.256[a]
Nesquehonite ($MgCO_3•3H_2O$)	−3.059[a]
Natron ($Na_2CO_3•10H_2O$)	−3.099[a]
Epsomite ($MgSO_4•7H_2O$)	−8.459[a]
Mirabilite ($NaSO_4•10H_2O$)	−6.288[a]
Halite (NaCl)	−5.592[a]
Magnesite ($MgCO_3$)	0
$Mg_3(PO_4)_2$	−8.465[a]
Thenardite ($NaSO_4$)	−8.263[a]

[a] Negative values indicate the solid is undersaturated in the aqueous system and is thus unable to precipitate.

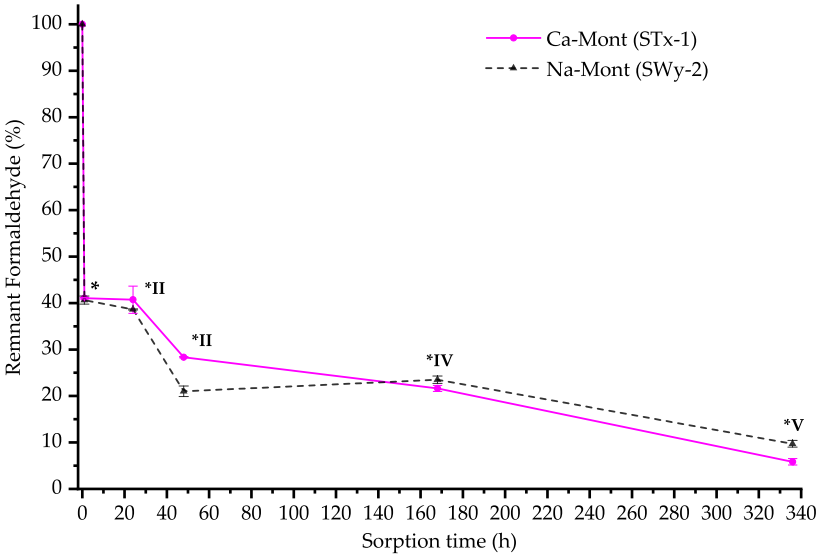

Fig. 5. Decomposition curve of formaldehyde under the experimental conditions as a function of sorption time.

derivatized aqueous supernatants exhibited several peaks that were identified by comparing their retention times to standard carbonyl–DNPH derivatives that were calibrated under the experimental conditions used in this study (Table 9). The aldehydes observed after sorption onto SWy-2 and STx-1 were identified as glycolaldehyde and glyoxal (Fig. 13c and 13d). The maximum concentration of these aldehydes in solution was reached at 336 h, although their formation was detected even at the lowest sorption times.

3.4. Clays in simulated ancient saline aqueous media

Following the sorption experiments, the Ca- and Na-montmorillonite (referred to as STx-1 and SWy-2, respectively) were analyzed using IR-ATR spectroscopy. An analysis of the 4000–2000 cm^{-1} and 2000–650 cm^{-1} regions revealed the presence of additional vibrational bands that were not originally present in the clay standards (Fig. 14). These bands were attributed to the vibrations of sp^3 carbons (Fig. 14a and b). The Si–OH vibrational band was notably deformed in the clay samples following sorption, which implies the presence of organic C–OH bonds (Fig. 14a and c). This data suggests that organic compounds were sorbed into the surface of the SWy-2 clays. In contrast, the spectra of the STx-1 clay before and after sorption did not exhibit any notable differences, suggesting that no organic matter sorbed onto these samples (Fig. 14c and d).

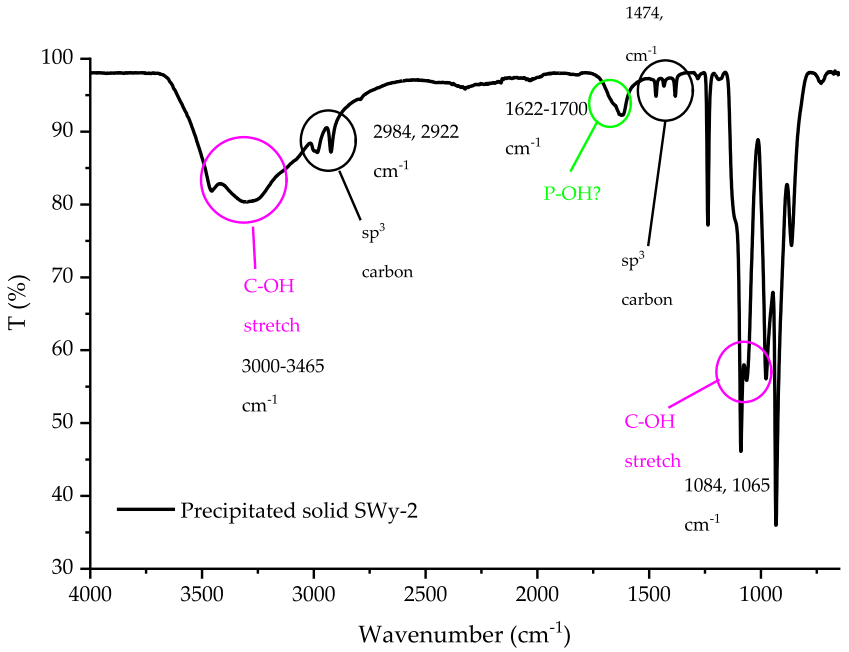

Fig. 6. The IR spectrum of the precipitated organic solids formed after sorption onto SWy-2 clay.

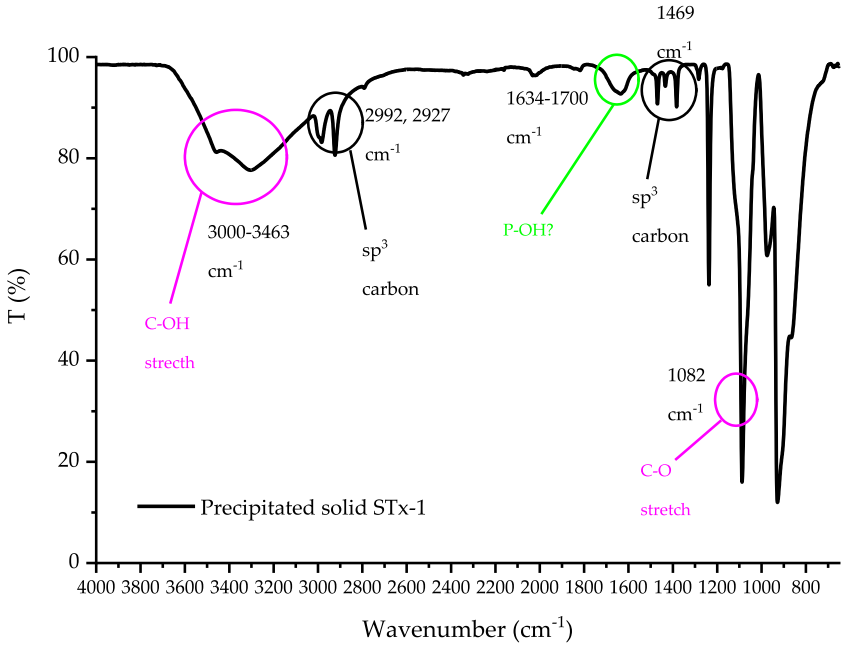

Fig. 7. The IR spectrum of the precipitated organic solids formed after sorption onto STx-1 clay.

3.5. *Quantification of the remaining phosphate in solution*

The total amount of phosphate in solution following sorption was calculated using an acid-base titration with 0.01 mol L^{-1} NaOH (Fig. 13). The initial phosphate concentration before sorption was calculated by titrating the initial formaldehyde saline solutions with the same reagent: this value was found to be 0.040 mol L^{-1}, representing the total amount of $H_2PO_4^{2-}$ available in the system for reaction with NaOH (additional phosphate species, formed by equilibrium with Mg and Na ions, were not accounted for in this study). The total percentage of phosphate (HPO_4^{2-}) in solution diminishes proportionally to sorption time, up to a maximum of 94 % and 80 % when exposed to SWy-2 and STx-1, respectively. At a pH of 6.0, the initial value used for the titration of the sample, the total

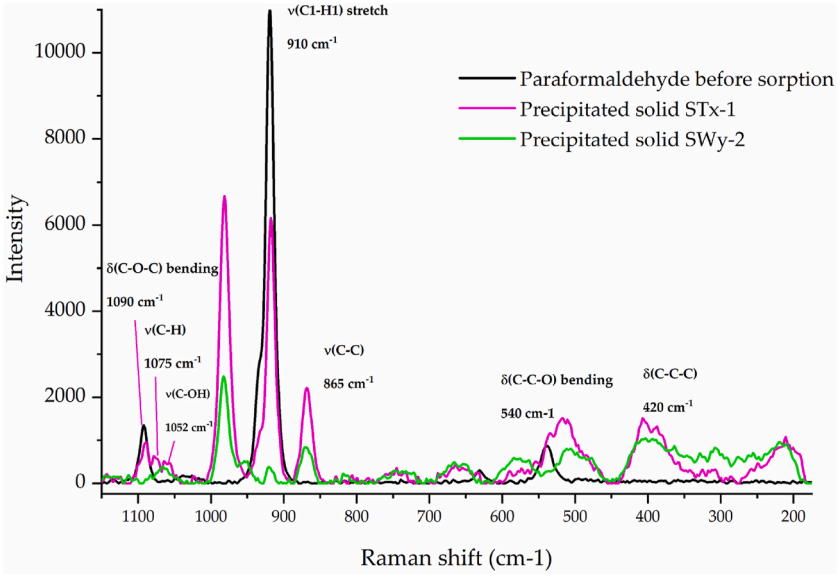

Fig. 8. Raman spectrum of the precipitated organic solids formed after sorption onto the clays used in this study (1150–800 cm^{-1} region).

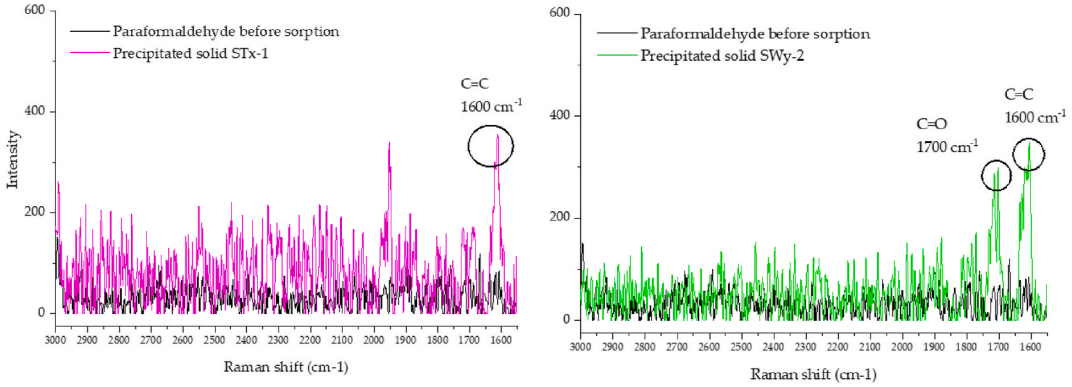

Fig. 9. Raman spectrum of the precipitated organic solids formed after sorption onto the clays used in this study (3000–1150 cm^{-1} region).

concentration of phosphate ion (HPO_4^{2-}) in our experimental system was 0.040 mol L^{-1}; i.e., final phosphate concentrations in solution were 0.037 and 0.032 mol L^{-1} for the systems exposed to SWy-2 and STx-1, respectively. The final concentration of phosphate in solution was reached at 48 h and remained stable up to the maximum sorption time (336 h)

4. Discussion

Formaldehyde and the formose reaction are chemical systems that are widely studied in prebiotic chemistry [6,34–36]. Most, if not all, of these studies focus on the role that formaldehyde plays as the main monomer in the aldol condensation reaction, which ends with the production of carbohydrates. The novelty of the present work is the insights that our experiments provide on the behavior of aldehydes in a simulated ancient saline system (specifically, alkaline 'soda' lakes). Soda lakes are considered to be promising settings for the occurrence of prebiotic reactions as they allow for the concentration of major elements as well as anions of biological relevance [37]. These lakes have been proposed as ideal environments in which phosphate could accumulate due to their concentration in water by the precipitation of its main sequestrant, Ca^{2+}, in the form of carbonates [16]. Lake Alchichica was selected as an analog of these ancient alkaline lake systems, as the hydrogeochemistry of the Alchichica system allows for the concentration of phosphate in a manner similar to the chemical equilibrium proposed in the cited references.

This was validated by studying the chemical equilibrium of the proposed experimental system. At modern temperature and CO_2 concentrations (25 °C and $pCO_2 = 3.5$ atm, respectively), the proposed hydrogeochemical model could accumulate up to 3.56×10^{-2} mol L^{-1} of phosphate in the form of HPO_4^{2-}. However, this accumulation was dependent on two factors: 1) the absence of microorganisms that could consume phosphate as nutrients [20], and 2) the absence of chemical cations with strong affinities for phosphate. The first condition is readily met in a prebiotic environment, as these systems would have been devoid of life. However, the second

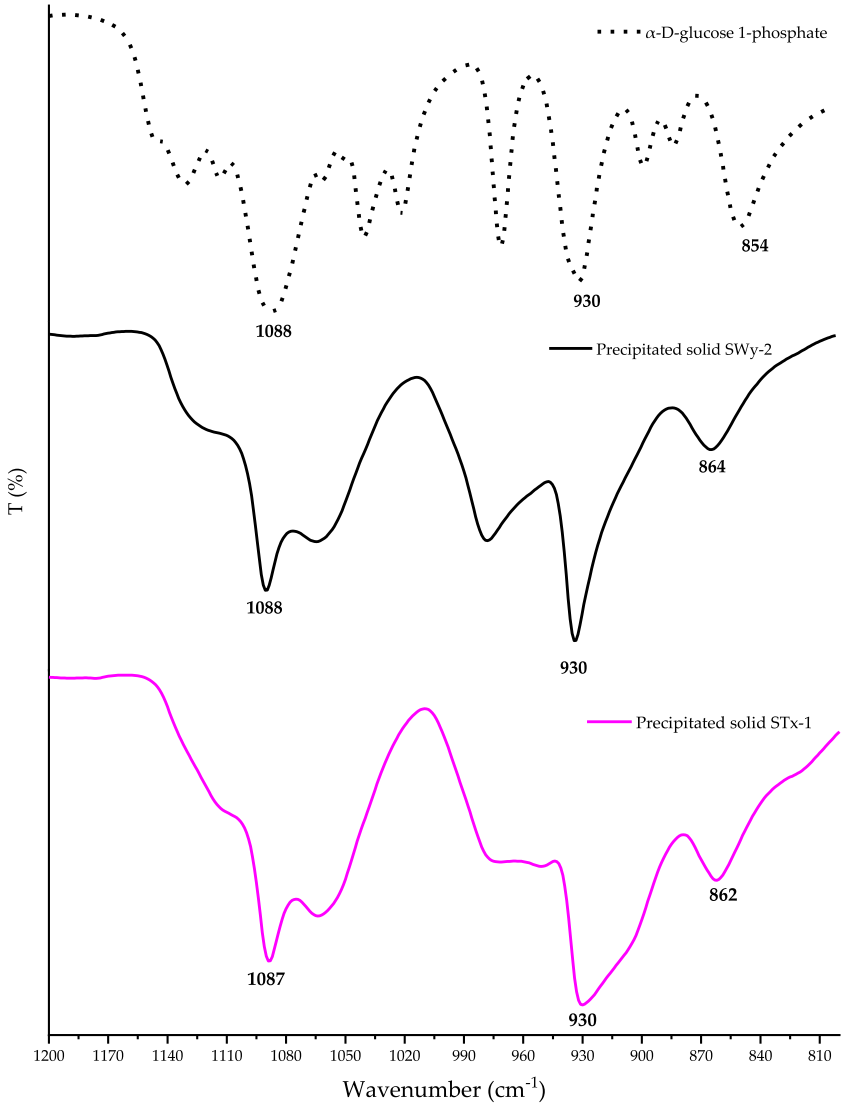

Fig. 10. The IR spectrum of the precipitated organic solids formed after sorption onto SWy-2 and STx-1 clays in the 1200–800 cm^{-1} region compared to α-D-glucose 1-phosphate standard. The 1088, 930, and 862 cm^{-1} bands are associated with the vibrational frequencies of phosphate groups [31].

condition depends entirely on the chemistry of the system, as the presence of ionic species that precipitate alongside phosphate, such as Ca^{2+}, Mg^{2+}, CO_3^{2-}, SO_4^{2-}, and F^-, could alter the precipitation equilibria of the systems [38,39]. The SI of all the possible mineral species under the Mg^{2+} and SO_4^{2-} concentrations of the simulated system can help determine if phosphate minerals are likely to precipitate. Table 4 shows that $Mg_3(PO_4)_2$ had an SI value of 0 under these conditions, indicating that it is in equilibrium with the system (*i.e.*, near saturation).

Modifying the temperature and CO_2 concentrations of the simulated saline waters to match the conditions proposed for the early Archean [29] resulted in changes in the phosphate and Mg^{2+} concentrations in the system (Table 5): dissolved phosphate concentrations were found to increase, while the concentration of Mg^{2+} decreased. This was due to the increase in the saturation of dissolved carbonate in the system as a result of the increase in pCO_2 due to the abundance of atmospheric CO_2. An analysis of the SI of the early Archean system reveals that magnesite ($MgCO_3$) was in equilibrium with these saline waters. Thus, the presence of a CO_2-rich atmosphere could have increased the chemical weathering rates of silicates, which, in turn, would have increased the amount of magnesium in solution. Although magnesite is the most thermodynamically stable form of magnesium carbonate, its precipitation is hindered at low ambient temperatures [40]. In contrast, the solubility of calcium carbonates would have been lower in highly alkaline systems. However, a high pCO_2 would have rapidly increased the precipitation rate of calcium carbonates, increasing calcite saturation in the system [41]. Consequently, the near saturation of magnesite in the system is primarily due to the absence of dissolved Ca^{2+}, which was likely sequestered by the precipitation of calcium carbonates.

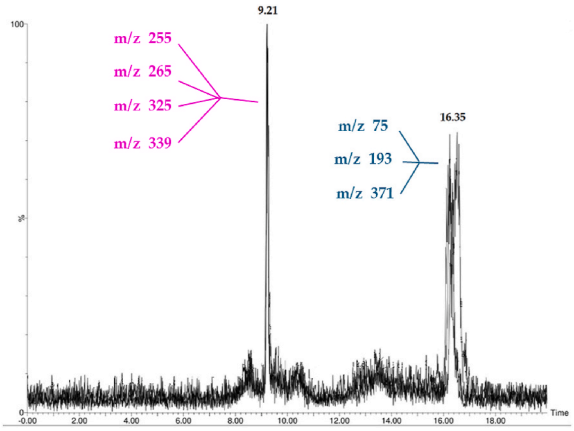

Fig. 11. a) Total ion count (TIC) HPLC-ESI-MS chromatogram of the sugar-like compounds detected in the sample supernatants following formaldehyde sorption onto SWy-2 in the simulated ancient saline lake solutions.

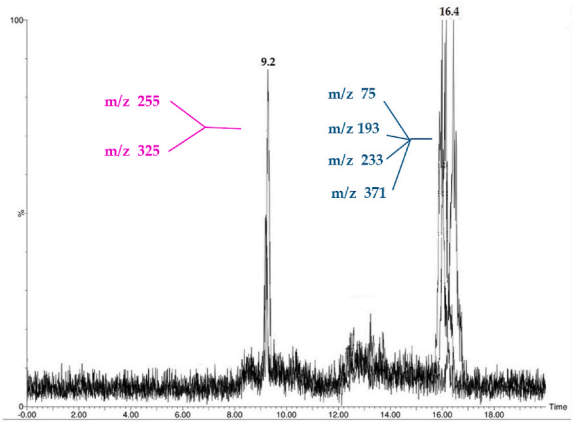

Fig. 12. a) Total ion count (TIC) HPLC-ESI-MS chromatogram of the sugar-like compounds detected in the sample supernatants following formaldehyde sorption onto STx-1 in the simulated ancient saline lake solutions.

Table 8
Elution times of standard carbohydrates in a GL Sciences® Inertsil NH_2 5 μm Column.

Compound	Elution time (min)
D-Glucose ($C_6H_{12}O_6$)	9.8 ± 0.03
D-Ribose ($C_5H_{10}O_5$)	7.97 ± 0.08
Sucrose ($C_{12}H_{22}O_{12}$)	11.37 ± 0.2

In the context of phosphate sequestration, the high affinity of magnesium for carbonate [40,41] would have favored the precipitation of magnesium carbonates over magnesium phosphate (Table 7), especially due to the high concentration of dissolved carbonate. In the simulated Archean alkaline water, the carbonate concentration was found to be the main control on phosphate concentration. Although magnesium weathering (and mobility) would have been higher, phosphate would still have accumulated because the precipitation of magnesium carbonates is thermodynamically favored, especially at increased pCO_2 values. Indeed, despite the near equilibrium of $Mg_3(PO_4)_2$ in modern simulated saline water, an increase in dissolved carbonate could lead to an increase in phosphate concentration in the system. This phenomenon has already been observed in Lake Alchichica, which possesses waters saturated in calcite, dolomite, and magnesite due to the high pCO_2 values in the environment. Phosphate is only undersaturated in the medium due to its consumption by local microorganisms [20]: this would not have been the case in a lifeless, early Archean environment in which only inorganic chemical species would have been capable of sequestering phosphate.

Formaldehyde was found to be labile under these experimental conditions, readily decomposing when exposed to SWy-2 and STx-1 clays (Fig. 5). The decomposition rate of the formaldehyde was independent of the type of clay. Previous studies have reported on the role that mineral surfaces play in the aldolic condensation of aldehydes; specifically, the mineral surfaces allow for the binding of the

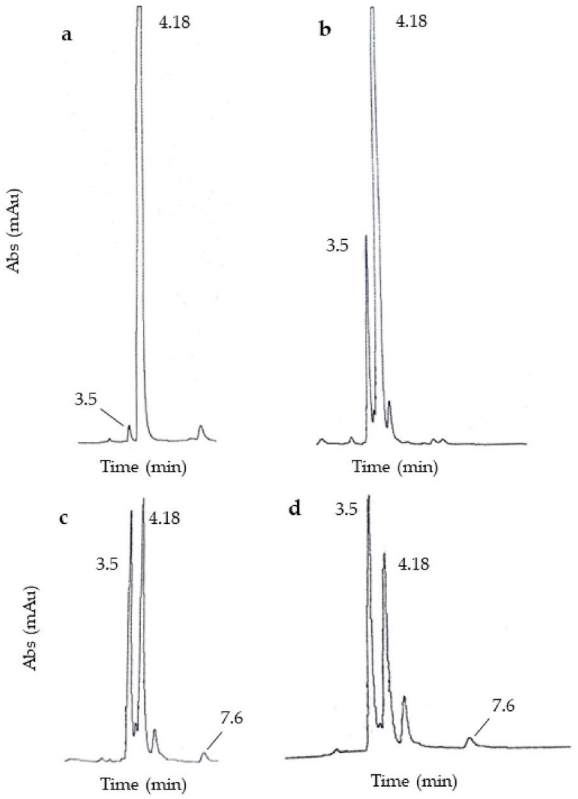

Fig. 13. HPLC chromatogram of sample supernatants derivatized with DNPH at different sorption times. a) Sample supernatant after 60 min of sorption onto STx-1. b) Sample supernatant after 60 min of sorption onto SWy-2. c) Sample supernatant after 336 h of sorption onto STx-1. d) Sample supernatant after 336 h of sorption onto SWy-2. Signals at retention times of 3.5, 4.18, and 7.6 min correspond to glycolaldehyde-DNPH, formaldehyde-DNPH, and glyoxal-diDNPH, respectively (Table 9). The small peak at 4.18 min corresponds to a glycolaldehyde impurity.

Table 9
Elution times of standard carbonyl-DNPH derivatives in a SUPELCO® Supelcosil LC C-18 Column.

Compound	Elution time (min)
Glyceraldehyde-DNPH	3.0
Glycolaldehyde-DNPH	3.4
Formaldehyde-DNPH	4.16 ± 0.3
Glyoxal-diDNPH	7.623 ± 0.7

OH groups of diols, enols, and enolates of aldehydes in solution onto clays under acidic and alkaline pHs [6,7,42,43]. Our experimental system was expected to exhibit similar behavior. An exhaustive analysis of the IR spectra of the SWy-2 and STx-1 clays before and after sorption yielded additional information about the chemical species bound to their mineral surfaces. Before sorption (Figs. 2 and 3), both clays exhibited bands associated with silica and surface OH groups (693, 797, 1633, and 3700–3400 cm^{-1}). A Fe^{3+} vibration band was detected (885 cm^{-1}) in the SWy-2 clay while vibrational bands corresponding to Al–OH (913 cm^{-1}) and Mg–OH (843 cm^{-1}) were detected in the STx-1 clay. An analysis of the chemical composition of both clays revealed that the primary difference between the SWy-2 and STx-1 clays was their Fe content [44], with SWy-2 possessing a maximum iron content of 4.37 % (in the form of Fe_2O_3) while STx-1 possessed a total Fe_2O_3 content of 1.20 %. The iron content of SWy-2 was thus high enough for the IR vibration band to overprint the Al–OH and Mg–OH bands. Following sorption, new IR bands appeared on the SWy-2 samples. Specifically, two absorption bands in the 2800–3000 cm^{-1} region, with an additional band appearing at approx. 700 cm^{-1} after 168 and 336 h of sorption with formaldehyde (Fig. 14). These vibration bands are associated with sp^3 carbons, which suggests that the decomposition products of formaldehyde had been bound to the surface of the clay. However, the mechanisms behind this binding process remain unknown. One potential mechanism for the sorption process is the binding of newly formed aldehyde enediolates, such as glycolaldehyde (Fig. 13), to Fe^{3+} cations [7], which, as shown earlier, are known to be present in higher concentrations in the SWy-2 clay compared to STx-1. However, further work is needed to correctly determine the mechanisms by which organic compounds are bound to the SWy-2 clay.

An exhaustive analysis of the IR and Raman spectra of the organic solids precipitated following the evaporation of water from the

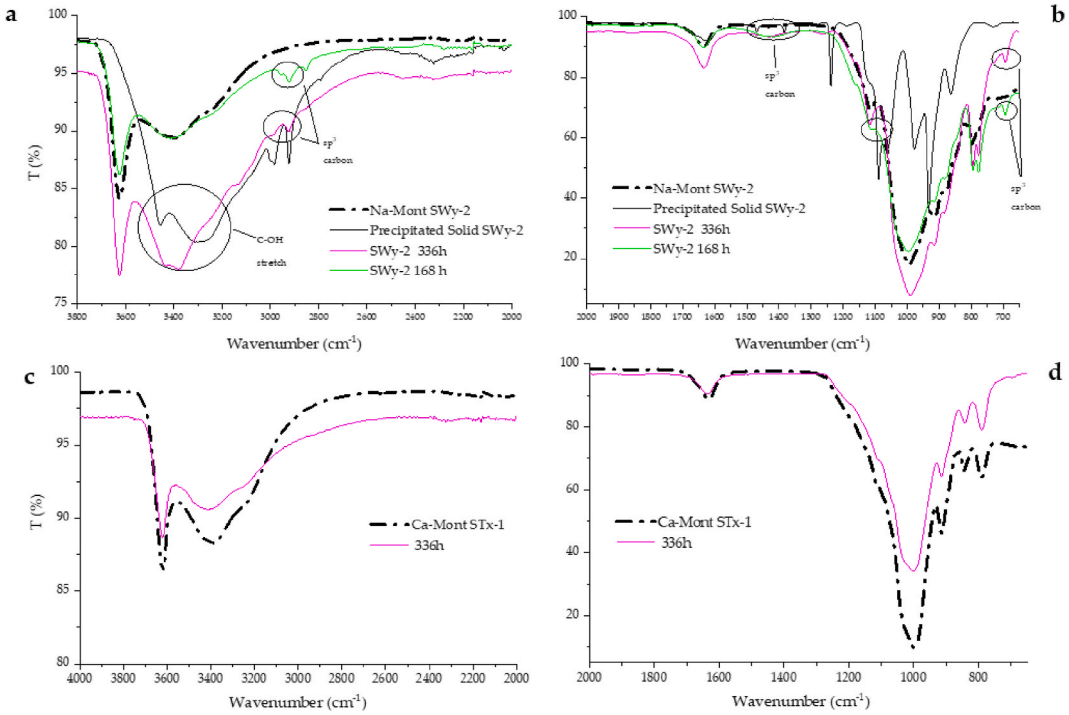

Fig. 14. IR spectra of the SWy-2 and STx-1 clay samples after sorption. Red circles indicate changes in the IR spectra compared to the original standards (black line). a) 4000–2000 cm^{-1} region of the SWy-2 sample. b) 2000–650 cm^{-1} region of the SWy-2 sample. c) 4000–2000 cm^{-1} region of the STx-1 sample. d) 2000–650 cm^{-1} region of the STx-1 sample.

experimental supernatants yielded useful information on the chemistry of the formaldehyde decomposition products (Fig. 6 and 7). Both IR spectra indicated the presence of C–OH, CH_3, and CH_2 functional groups. The IR spectra of the precipitated solids obtained after sorption onto STx-1 revealed the presence of a vibrational band associated with C–O stretching, in contrast, the IR spectra of the sample exposed to SWy-2 exhibited bands associated with the C–OH stretching of secondary alcohols. These results indicated that the precipitated solids from both samples were primarily composed of a mixture of molecules containing R–OH and C–O–C functional groups. Raman spectroscopy and ESI analysis were conducted to further investigate the structure of these compounds.

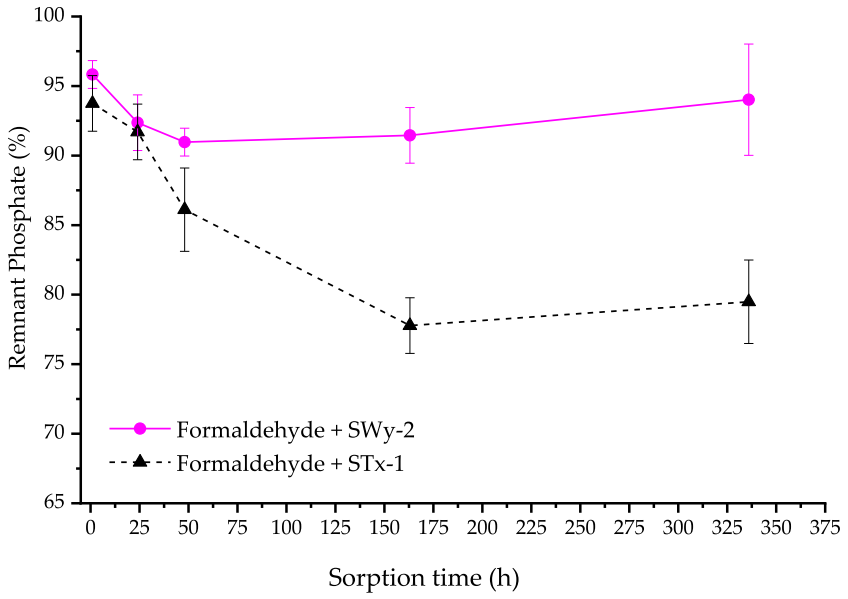

Fig. 15. Remaining phosphate in solution after sorption with SWy-2 and STx-1 clays.

The Raman spectra of the samples exhibited notable differences compared to the paraformaldehyde standard used for sample preparation (Figs. 8 and 9); specifically, they contained evidence of vibrational bands associated with the vibrational modes of C–C–O, C–O C, C=O, C–C–C, and C–H bonds. By analyzing the Raman spectra of commercial analytical grade D-Glucose (Fig. 15 and 16), we attributed the detected vibrational bands to the presence of glucose isomers such as α or β-glucose (Fig. 16a and c) [45]. The vibrational bands between 910 and 848 cm^{-1} (Fig. 16b) are often associated with glucose isomers. Most of the bands associated with the vibrational modes of glucose functional groups are present in the precipitated solids of both samples (Fig. 17). In the 1600-1200 cm^{-1} region (Fig. 17a), the CH_2, δ(O–C–H), δ(C–C–H), and υ(C–O) stretching modes exhibited similar spectra profiles and wavenumber values to the glucose standard as well as to values reported in the literature [45]. Bands at 848 and 916 cm^{-1} (Fig. 17b) are commonly associated with υ(C–C) and δ(C1–H1) vibrations in α-glucose, while these bands are shifted to 868 and 916 cm^{-1} for β-glucose [45]. A shift from 848 cm^{-1} to 865 cm^{-1} was observed in both precipitates, consistent with the υ(C–C) vibration of β-glucose. However, the vibration band associated with the υ(C–H) vibration (894 cm^{-1}) was notably absent, suggesting that the precipitated solids were neither α- nor β-glucose, but instead a complex mixture of sugar-like cyclic and linear polyalcohols and ethers with chemical structures similar to those of glucose. This was further supported by the absence of the endocyclic δ(C–C–O) vibration at 450 cm^{-1} (Fig. 17c), implying the presence of linear pentoses and hexoses in the sample. The lack of this band, as well as the low intensity of the vibration bands in the 1200–1000 cm^{-1} region, where the signals of the δ(C–O–C) angle bending mode typically appear, further suggests the

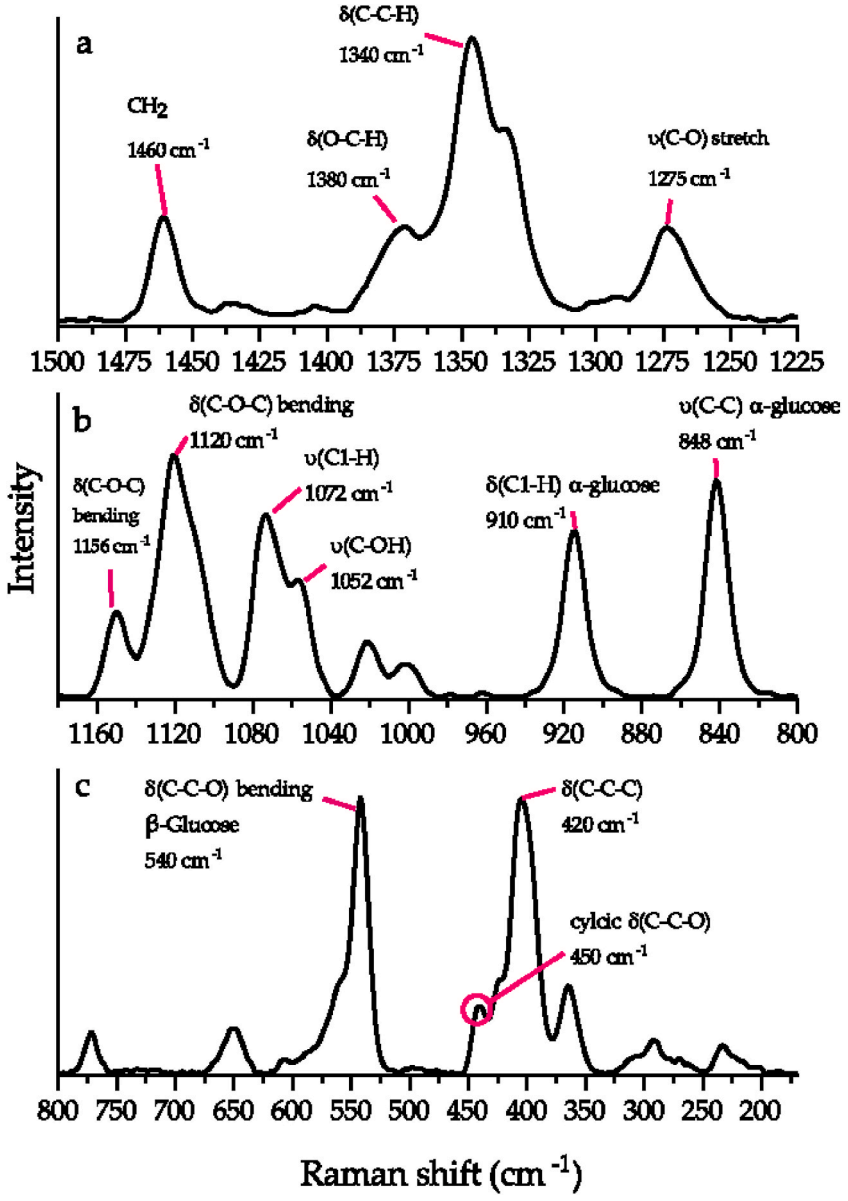

Fig. 16. The Raman spectrum of glucose standards. a) 1500–1225 cm^{-1} region; b) 1200–800 cm^{-1} region; c) 800–150 cm^{-1} region.

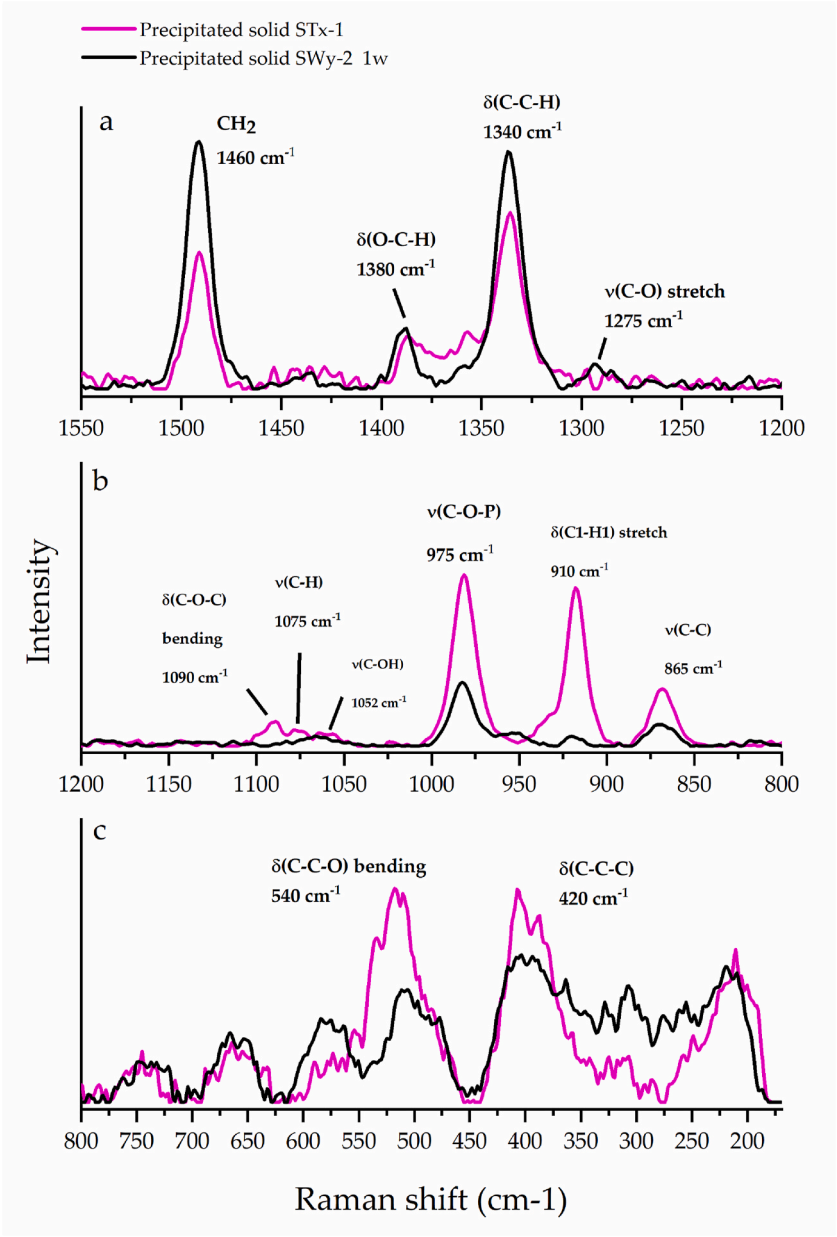

Fig. 17. Raman spectrum of precipitated solids after sorption with SWy-2 and STx-1 clays. a) 1600–1200 cm^{-1} region; b) 1200–800 cm^{-1} region; c) 800–150 cm^{-1} region.

absence of cyclic sugar-like compounds.

A new band at approximately 975 cm^{-1} appeared after sorption (Fig. 18). This band was not present in the Raman spectrum of formaldehyde before sorption but was observed in the α-D-glucose 1-phosphate spectrum. This band was thus identified as being associated with the antisymmetric C–O–P stretching vibration of phosphorylated organic compounds [32,33]. An analysis of the IR spectrum of the samples revealed more information about the nature of the phosphate groups present in the experimental samples. As previously mentioned, diagnostic phosphate peaks typically appear between 1300 and 800 cm^{-1} [31]. These peaks are shown in a non-aqueous physical mixture of glucose with disodium hydrogen phosphate heptahydrate, where the unreacted phosphate peak values are shown (Fig. 19b). The spectrum of disodium hydrogen phosphate heptahydrate (Fig. 19c) highlights the presence of monoprotonated phosphate (HPO_4^{2-}) at 1050 and 869 cm^{-1}, which can also be found in the SWy-2 and STx-1 organic precipitates (Fig. 19d and e). These bands were shifted to higher (1088 cm^{-1}) and lower (845 cm^{-1}) values, respectively, compared to the vibration bands present in the α-D-glucose 1-phosphate spectrum (Fig. 19a), which also exhibited a band of 930 cm^{-1}, associated with a separate phosphate vibration mode. The absence of the 930 cm^{-1} signal in the pure disodium hydrogen phosphate heptahydrate spectrum

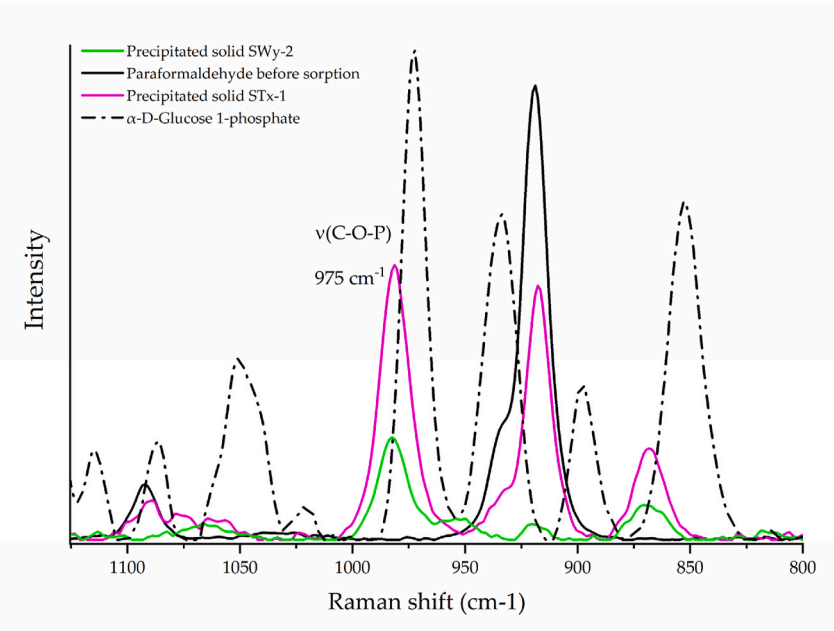

Fig. 18. Comparison between Raman spectra in the 1125–800 cm^{-1} region, in which the vibrational band characteristic of υ(C–O–P) appears.

suggests this is a vibration band unique to organically bound phosphate. Organophosphate bands could also be observed in the SWy-2 and STx-1 organic precipitates, indicating that these samples likely contained some amount of phosphorylated compounds as well as a significant quantity of unreacted disodium phosphate. The exact structure of these compounds is unknown; however, we can assume that they are composed of a mixture of both linear and cyclic sugar-like compounds based on the Raman analysis. If phosphorus-containing compounds were indeed formed, this suggests that the decrease in the dissolved phosphate concentration was due to phosphorylation reactions (Fig. 15). In this case, the maximum concentration in solution would have been 3×10^{-3} and 8×10^{-3} mol L^{-1} for the SWy-2 and STx-1 clays, respectively. It should also be assumed that not all of the available phosphate would have reacted with the available organic material, as some of it could have been sorbed by the clays. However, the spectroscopic analysis of the clay samples did not reveal the presence of any phosphate groups bound to the mineral surface, suggesting that most of the phosphate must have reacted with the available organic compounds in solution.

As a complementary analysis, possible phosphorylated compounds in the experimental samples were identified using HPLC-RI (refraction index) and ^{31}P NMR. The chromatogram of the supernatants from the experimental samples after 336 h of sorption with SWy-2 and STx-1 clays (Fig. 20c and d, respectively). Two different compounds with a retention time of 8.5 and 10.1 min were identified: the retention time of the first compound matched that of α-D-glucose phosphate, a phosphorylated standard (Fig. 20a), indicating that this compound was a phosphorylated molecule with chemical characteristics that closely resembled that of this standard. This analysis also confirmed the presence of remnant HPO_4^{2-} (Fig. 20b) that had been previously detected by IR spectroscopy. When a 1:1 mixture of the phosphorylated standard and the experimental samples was analyzed through co-injection (Fig. 20e and f), the intensity of the compound increased, while its peak shape and retention time remained constant for both clay samples. ^{31}P Nuclear magnetic resonance (^{31}P NMR) of the precipitated organic solids (Fig. 21) confirms the presence of one phosphorylated compound in each sample analyzed by this technique. The chemical shifts at 2.5 (Figs. 21a) and 2.2 (Fig. 21b) ppm suggests that the phosphorylated compound detected could be a phosphate ester [46–49].

Electrospray ionization was used on the supernatants obtained from the SWy-2 (Fig. 11) and STX-1 (Fig. 12) samples to correctly determine the molecular weight and likely chemical formula of the decomposition products. Both chromatograms revealed the presence of two different compounds with retention times of 9.21 and 16.35 min. The product ion mass spectrum of $[M - H]^-$ (derived from formaldehyde) for each chromatographic peak revealed a rather complex ion spectrum. The analysis of the sugars and sugar-like compounds using negative ion ionization modes revealed a significant amount of fragmentation products [50]. Monosaccharides and oligosaccharides tend to fragment when analyzed without derivatization [51]. IR and Raman spectra show that the main functional groups of the decomposition products are C–O–C, C–OH, C–C, C=O, and C=C. Consequently, we can infer that the product ion mass spectrum is composed primarily of polyethers and polyalcohols with similar polarities that are not easily separated using silica-bonded NH_2 HPLC columns, as well as the fragmentation products of large linear or cyclic sugar-like molecules.

The most abundant ions $[M - H]^-$ detected at 9.2 and 16.3 min in the SWy-2 and STx-1 samples, as well as their proposed chemical formulas, are presented in Tables 10 and 11, respectively. It should be noted that the proposed chemical formulas are not definitive, as the complex nature of the samples as well as the presence of multiple isomers means that the *m/z* of the observed ions can be described by more than one chemical formula. When analyzed by electrospray ionization in negative mode, sugars (monosaccharides and polysaccharides) fragment into ions that are characterized by the loss of H_2O (*m/z* 18) and CH_2O (*m/z* 30) [50–52]. Consequently, we

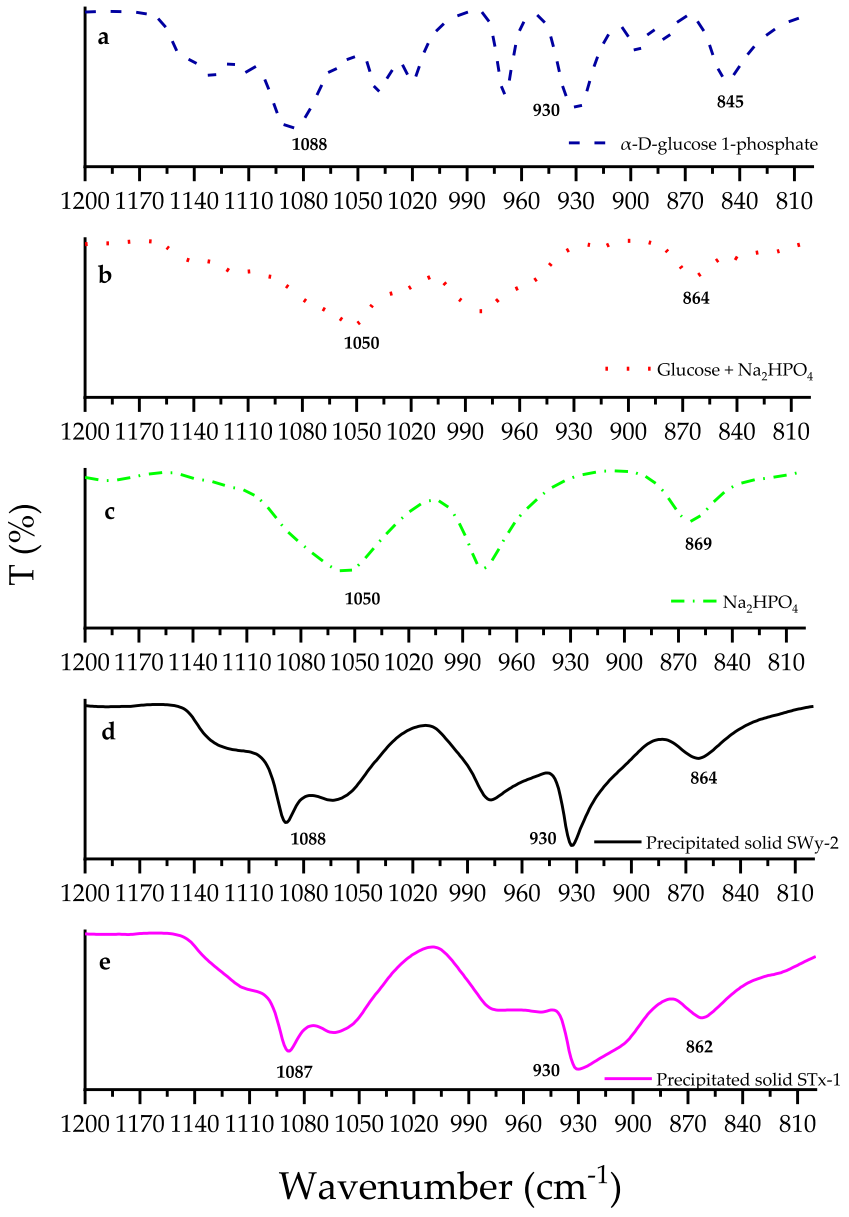

Fig. 19. IR spectra (1200–750 cm^{-1} region) of precipitated organic solids after sorption. a) IR spectra of α-D-glucose 1-phosphate. b) IR spectra of the homogenized mixture. c) IR spectra of disodium phosphate heptahydrate. d) IR spectra of precipitated organic solid after sorption onto SWy-2 clay. e) IR spectra of precipitated organic solid after sorption onto STx-1.

can assume similar fragmentation patterns and chemical behavior in sugar-like compounds (including both cyclic and linear molecules) as they are isomers of sugars. We propose that the ions at *m/z* 371 and 185, which were detected in both samples at 16.3 min, are the result of the loss of H_2O and CH_2O from $C_{13}H_{26}O_{13}$. m/z 371 corresponds to the loss of a single H_2O fragment, while *m/z* 185 corresponds to the loss of two CH_2O fragments and one H_2O fragment. The ion at *m/z* 233 could be a fragment resulting from the loss of two H_2O fragments from $C_9H_{18}O_9$. These ions eluted at high retention times, suggesting that they are the products of cyclic or linear sugar-like compounds of high molecular weight since it is well-known that monosaccharides are rapidly eluted in silica-bonded NH_2 columns [53]. Ions with $m/z < 340$ could be the products of several different polyalcohol or polyether compounds (i.e., CHO compounds). These compounds are expected to elute first as they are not strongly retained in NH_2 columns and are thus more abundant at lower retention times.

HPLC-UV analysis revealed the presence of both glycolaldehyde ($C_2H_4O_2$) and glyoxal ($C_2H_2O_2$) in solution after sorption onto both clay species. Both molecules were present in relatively low concentrations (compared to formaldehyde) after the minimum amount of sorption time (60 min); a sharp increase in concentration was observed after 336 h. The detection of both aldehydes suggests that the main mechanism by which these sugar-like and CHO compounds were formed could be base-catalyzed aldol condensation [54] via

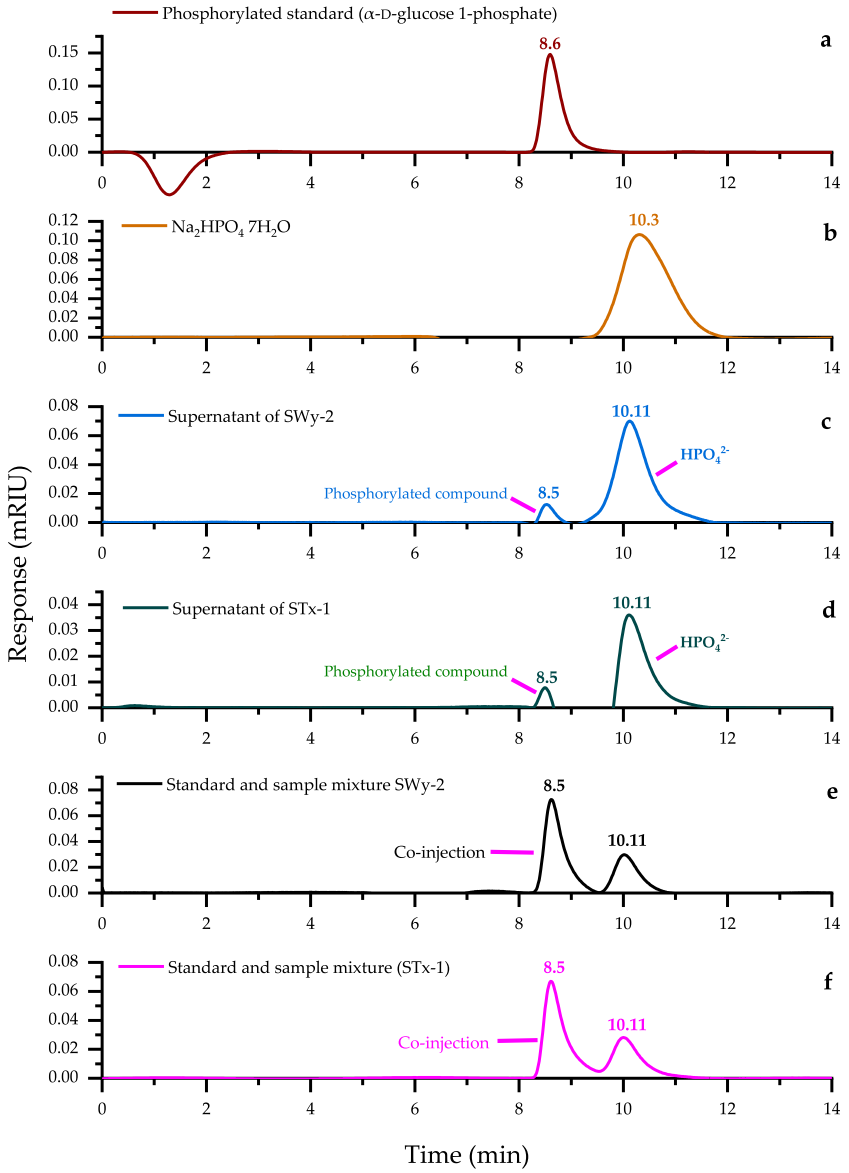

Fig. 20. HPLC chromatogram of phosphorylated compounds. a) α-D-glucose 1-phosphate. b) Na_2HPO_4 $7H_2O$ salt. c) Supernatant of samples after sorption onto SWy-2. d) Supernatant of samples after sorption onto STx-1. e) Co-injection of phosphorylated standard (α-D-glucose 1-phosphate) with supernatant of samples after sorption onto SWy-2. f) Co-injection of phosphorylated standard (α-D-glucose 1-phosphate) with supernatant of samples after sorption onto STx-1.

formaldehyde polymerization. Indeed, glycolaldehyde has been characterized as an important intermediary in this type of reaction [55]; consequently, its detection in the experimental samples supports aldol condensation as the primary mechanism by which CHO compounds are formed. Glycoaldehyde (and other aldehyde intermediates) is initially produced by formaldehyde polymerization (Fig. 13a and b) and consumed until almost all of the initial formaldehyde is transformed into CHO and sugar-like compounds (Fig. 13c and d). Although glycolaldehyde is principally an intermediary, it remains in solution due to its stability; furthermore, its resonant form, glyoxal, reduces its reactivity to enol addition. The detailed mechanisms of the aldol condensation reaction can be found in multiple studies [6,34,36,43]. Scheme 1 presents a theoretical reaction mechanism through which sugar compounds could form in this experimental system under these conditions. In this proposed scheme, formaldehyde condenses into glycolaldehyde which subsequently condenses into glyceraldehyde. The keto-enol equilibrium favors retro-aldol condensation, resulting in the formation of sugar molecules: the sugar-like compounds observed in this study could have followed a similar formation pathway. In addition, the alkaline conditions could have catalyzed the condensation of formaldehyde-diol ($CH_2(OH)_2$) into the CHO compounds [56] as shown in Scheme 2.

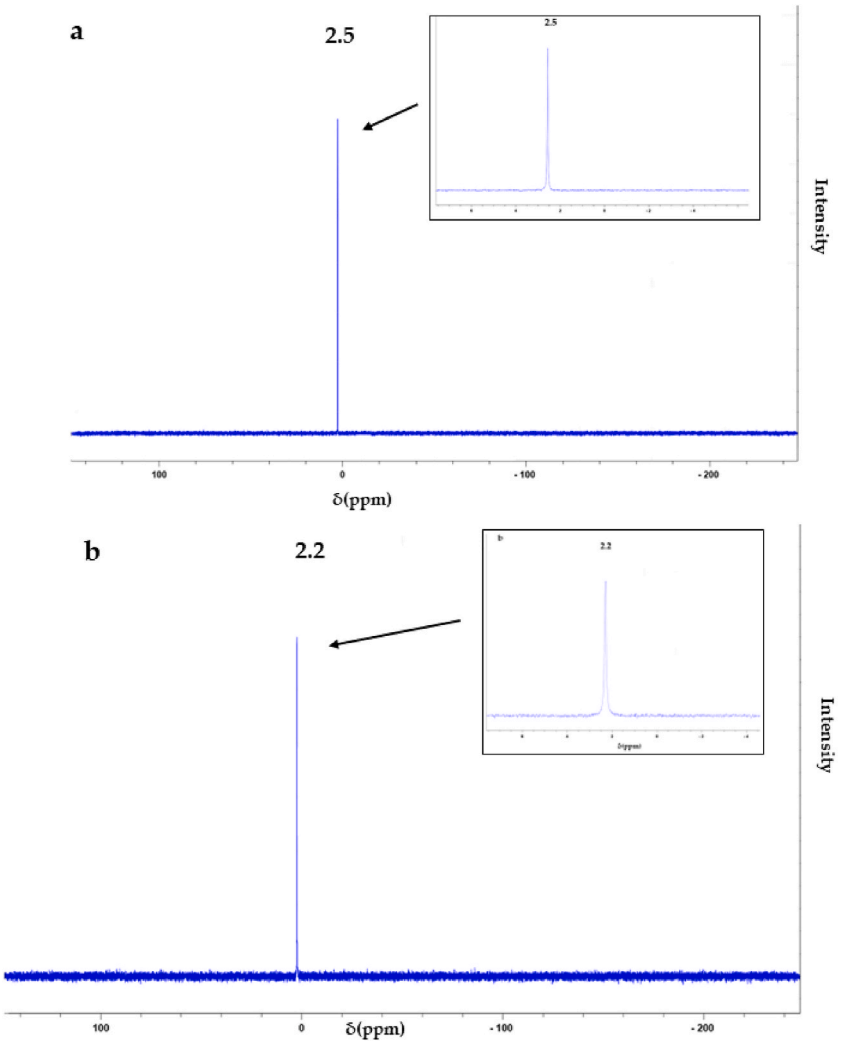

Fig. 21. ^{31}P NMR spectra of precipitated organic solids after sorption with a) SWy-2 clay and b) STx-1 clay. A single phosphate peak in each sample is located at 2.5 and 2.2 ppm, which are associated with the presence of a single phosphate ester in the precipitated organic solids.

Table 10
m/z of the most abundant ions in the samples sorbed onto SWy-2 clays.

RT 9.2 min			RT 16.35 min		
Observed *m/z* ([M − H]$^-$)	Molecular weight (g mol^{-1})	Probable chemical formula	Observed *m/z* ([M − H]$^-$)	Molecular weight (g mol^{-1})	Probable chemical formula
255	256	$C_9H_{20}O_8$	75	76	$C_3H_8O_2$
265	266	$C_{12}H_{26}O_6$	193	194	$C_7H_{14}O_6$
325	326	$C_{14}H_{30}O_8$	371	372	$C_{13}H_{24}O_{12}$
339	340	$C_{15}H_{32}O_8$			

4.1. Implications for prebiotic chemistry

The analysis of the decomposition products of formaldehyde at pH 9.13, 298 K, and in solution with Na^+, Cl^-, HPO_4^{2-} rich waters with no dissolved O_2 revealed that the primarily chemical species formed are composed of CHO-containing compounds and sugar-like molecules. The rate of formation of these compounds is slow, requiring up to 24 h to synthesize detectable organic compounds. After 60 min of sorption, the remnant formaldehyde in solution is approximately 50 %. Following this initial period, the decomposition rate slows significantly, reaching a maximum of 90 % at 336 h. Reactions in the presence of SWy-2 and STx-1 clay resulted in the same products. There was no discernible difference between the reaction products formed across the different clay species; this was expected

Table 11
m/z of the most abundant ions in the samples sorbed onto STx-1 clays.

RT 9.2 min			RT 16.04 min		
Observed *m/z* ([M − H]$^-$)	Molecular weight (g mol^{-1})	Probable chemical formula	Observed *m/z* ([M − H]$^-$)	Molecular weight (g mol^{-1})	Probable chemical formula
255	256	$C_9H_{20}O_8$	75	76	$C_3H_8O_2$
325	326	$C_{14}H_{30}O_8$	175	176	$C_7H_{12}O_5$
			233	234	$C_9H_{14}O_7$
			371	372	$C_{13}H_{24}O_{12}$

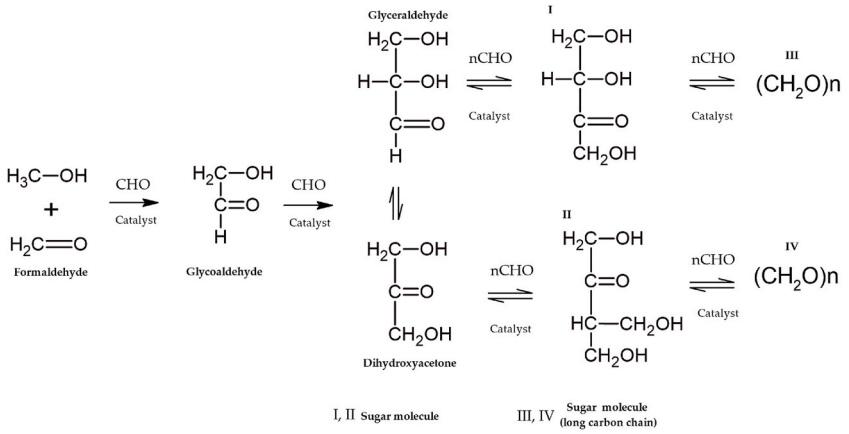

Scheme 1. Formation of sugar-like compounds.

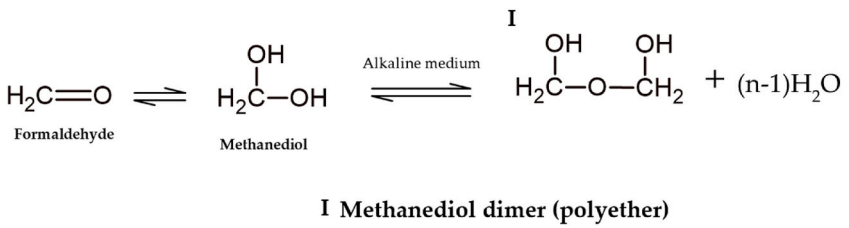

Scheme 2. Formation of CHO compounds.

as both clays possessed similar chemical compositions.

Although the type of clay did not influence the type of CHO compounds and sugar-like molecules formed in the simulated saline waters, it did affect the speed of formation of these chemical species. Fig. 22 shows the detection of sugar-like compounds by HPLC-ELSD on the experimental samples. When a solution of formaldehyde and saline water was left to react without clays, no chemical species were detected (Fig. 22a). In contrast, sugar-like compounds were detected when formaldehyde was dissolved in MiliQ grade water and allowed to adsorb onto the SWy-2 and STx-1 clays (Fig. 22b and c). Additional sugar-like and CHO chemical species were observed when clay was added to the system (Fig. 22d and e). This data suggests that the clays and the dissolved ions in solution act as catalysts for aldol condensation reactions. Under alkaline conditions, both the OH^- ion and the R–OH mineral groups can act as catalysts for formaldehyde by deprotonating the α-carbon and favoring the condensation of formaldehyde units. Divalent cations can also act as catalysts [43]. The combination of both divalent cations (Ca^{2+}, Mg^{2+}) and the hydroxyl groups on the mineral surfaces of the clays would thus have catalyzed aldol condensation reactions. The apparent sorption of organics onto the SWy-2 clays (and lack thereof, in the case of STx-1) suggests that hydroxy groups catalyze the condensation reaction when formaldehyde binds to SWy-2 clay. Since STx-1 is slightly richer in divalent cations, condensation could have occurred in the aqueous medium. However, it is important to note that although aldol condensation reactions could have occurred, the formation of biologically relevant sugars, such as ribose or pentose, was not detected. None of the ions observed in the ESI-MS spectra were associated with the known *m/z* of biologically relevant sugars (e.g., 149 and 179). This is because the formation of ribose and glucose by aldol condensation reactions requires extremely high initial concentrations of formaldehyde as well as high-temperature conditions. Even then, without the presence of specific mineral phases—such as borate and molybdate (which inhibit the retro-aldol degradation of formed sugars [6])— these important bio-molecules are unlikely to accumulate in an experimental system. Consequently, the formation and accumulation of ribose and pentose seems unlikely in our laboratory-based simulated ancient saline water samples, especially when clays as the only mineral phase

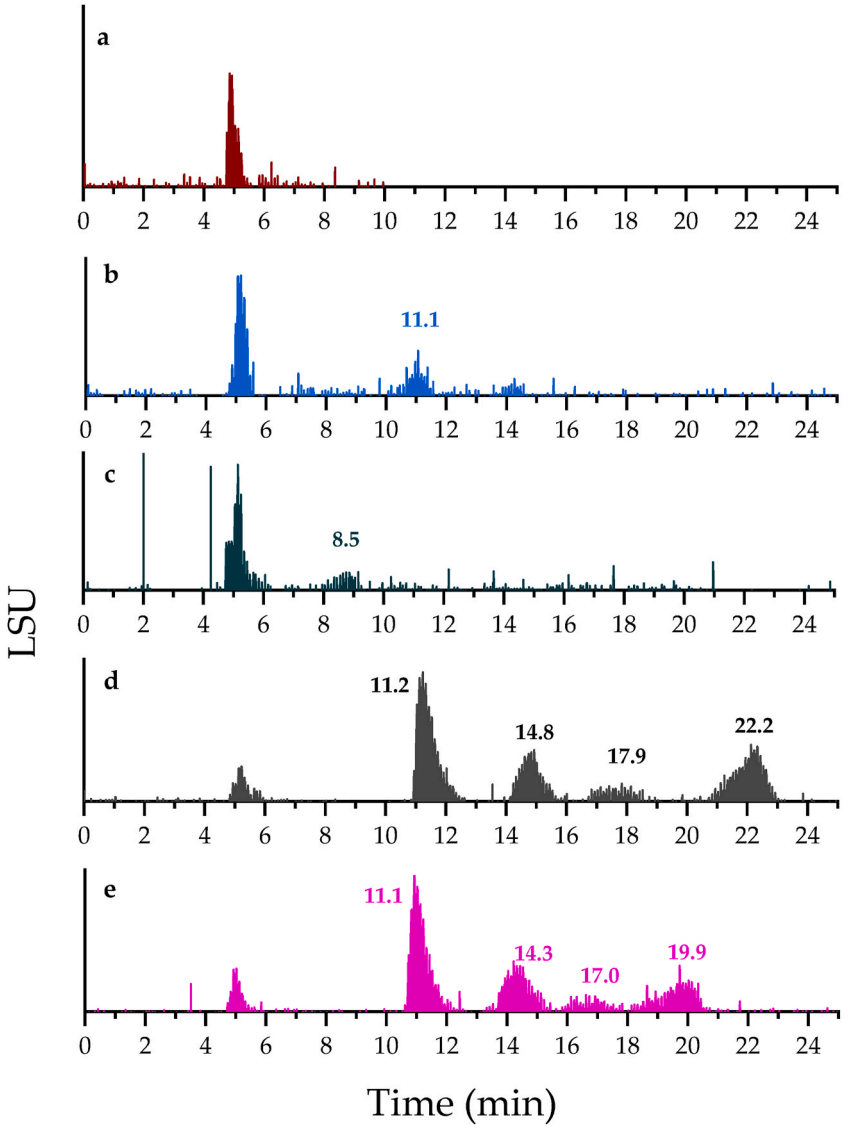

Fig. 22. HPLC chromatogram of sample supernatants analyzed after sorption onto SWy-2 and STx-1 clays. a) Formaldehyde in saline water after 336 h. b) Formaldehyde dissolved in MiliQ water after sorption onto SWy-2. c) Formaldehyde dissolved in MiliQ water after sorption onto STx-1. d) Formaldehyde dissolved in saline water after sorption onto SWy-2. e) Formaldehyde dissolved in saline water after sorption onto STx-1. The compound at a retention time of 5 min represents an impurity present in MiliQ water.

present.

Our theoretical calculations show that HPO_4^{2-} is freely available to react in the system. When the pCO_2 values increase to levels proposed for the early Earth, the phosphate ion is capable of accumulating in ancient saline lakes that have physicochemical characteristics similar to those found in our simulated system. The spectroscopic and chromatographic analysis of the samples suggests that phosphorylated organic compounds could have formed in this experimental system. However, the mechanism behind their formation remains elusive. Previous studies have suggested that systems with low water activity ($a_w < 1$) may drive the phosphorylation of organic compounds [15,57,58]. a_w diminishes when solute concentrations increase [59]. When a mixture of salts is present, the total loss of a_w in the system is equal to the sum of the loss of water activity that can be attributed to each solute in the system [60]. Our experimental system contains multiple solutes (e.g., Na^+, Mg^{2+}, Cl^-, SO_4^{2-}, HPO_4^{2-} and CH_2O), with the most highly concentrated solutes being Na^+ (0.12 mol L^{-1}) and CH_2O (1.5. mol L^{-1}) [61]. reported that solutions with Na and organic solutes (sucrose/D--glucose) at concentrations close to those reported in our system result in a_w values of 0.997 and 0.975, respectively. Consequently, our system is expected to have an a_w value of <1, which could be the main factor that drives phosphorylation in early Archean waters. Alternatively, water evaporation could be the main driver of phosphorylation. As water is removed from the system, the equilibrium of the phosphorylation reactions is displaced towards its products in response to the removal of water. Water evaporation could occur in

saline lakes, as their hydrological regime is dependent on cycles of evaporation and precipitation [38]. If phosphorylation reactions are truly occurring in our system, this would suggest that ancient saline lakes could not only be environments in which phosphate could have accumulated but also systems in which the high solute concentration would have driven the sequestration of available phosphate by organic compounds, if any were available.

5. Conclusion

The condensation of formaldehyde under alkaline conditions is often considered to be a "messy" system as it results in the formation of a wide variety of sugars and sugar isomers. It is also affected by several factors, including temperature, the presence of specific mineral phases, solute concentrations, and pH [55]. Our work shows that the following phenomena occur in a system that closely resembles the physicochemical conditions that can be encountered in a natural ancient environment (i.e., an alkaline saline lake).

1. Formaldehyde readily decomposes in the presence of Ca and Na montmorillonite into sugar-like and CHO-containing compounds that are formed by base-catalyzed aldol reactions and formaldehyde-methanediol condensation, respectively.
2. The complex nature of the aldol condensation reactions does not allow for the formation of sugars of biological importance (e.g., ribose, glucose) under these experimental conditions. Although clays could catalyze the decomposition and condensation of formaldehyde, they do not allow for the "chemical selection" of those sugars. Consequently, in a theoretical, primitive environment whose characteristics match those of the proposed experimental system, sugar formation and accumulation appear to be unlikely.
3. Our analysis (^{31}P NMR, Raman spectroscopy, IR spectroscopy and HPLC) suggests that phosphorylation reactions could have occurred in ancient saline lakes. These reactions could have occurred due to the low a_w of the environment (due to high salinity), water evaporation, or both.
4. Lake Alchichica can be considered an analog of ancient saline lakes as its chemical and mineralogical composition allows for the accumulation of phosphate, especially at atmospheric and temperature conditions that match those associated with the early Archean (3.8 Ga). Saline and soda lakes are interesting and novel environments in which prebiotic reactions could have occurred in the early Earth.

Ethical statement

This work does not involve the use or animal of human subjects.

Funding

This work was supported by CONACHyT fellowship 319818 and PAPIIT grant IN114122.

Data availability statement

The data generated and analyzed during the current study is included in the body of this paper. Additional data, if required, will be made available upon request.

CRediT authorship contribution statement

Claudio Alejandro Fuentes-Carreón: Writing – review & editing, Writing – original draft, Visualization, Methodology, Formal analysis, Conceptualization. **Adriana Leticia Meléndez-López:** Writing – review & editing, Methodology, Investigation, Formal analysis, Data curation. **Jorge Armando Cruz-Castañeda:** Writing – review & editing, Writing – original draft, Formal analysis, Data curation. **Alicia Negrón-Mendoza:** Writing – review & editing, Supervision, Resources, Project administration, Investigation, Funding acquisition, Conceptualization.

Declaration of competing interest

The authors declare that they have no known competing financial interests or personal relationships that could have appeared to influence the work reported in this paper.

Acknowledgements

The authors acknowledge the support of the Instituto de Ciencias Nucleares at the Universidad Nacional Autónoma de México (UNAM) and Posgrado en Ciencias de la Tierra. The authors acknowledge the funding CONACHyT fellowship 319818 and PAPIIT grant IN114122. The authors wish to thank M. Sc. Gerardo Cedillo Valverde for his technical assistance. The authors are grateful to C. Claudia Camargo Raya for her technical assistance in the Laboratorio de Evolución Química, ICN-UNAM; Dr. Karina Elizabeth Cervantes de la Cruz, Dr. Alejandro Heredia Barbero, Dr. Maria del Carmen Virginia Ortega Alfaro and Dr. Saul Alberto Villafañe Barajas for their invaluable academic assistance and guidance throughout the experimental process. We are also grateful to Mr. José Rangel

Gutierrez, Mr. Martín Cruz, and Mr. Enrique, M.Sc. for their contributions. Finally, the authors are grateful to the reviewers involved in the revision process, as their suggestions helped improved the quality of the present work.

References

[1] A. Yamagishi, T. Kakegawa, T. Usui (Eds.), Astrobiology: from the Origins of Life to the Search for Extraterrestrial Intelligence, Springer Singapore, Singapore, 2019, https://doi.org/10.1007/978-981-13-3639-3.
[2] S.L. Miller, A production of amino acids under possible primitive earth conditions, Science 117 (1953) 528–529, https://doi.org/10.1126/science.117.3046.528.
[3] P. Dalai, H. Kaddour, N. Sahai, Incubating life: prebiotic sources of organics for the origin of life, ELEMENTS 12 (2016) 401–406, https://doi.org/10.2113/gselements.12.6.401.
[4] A. Butlerow, Bildung einer zuckerartigen Substanz durch Synthese, Justus Liebigs Ann. Chem. 120 (1861) 295–298, https://doi.org/10.1002/jlac.18611200308.
[5] O. Botta, J.L. Bada, Extraterrestirial organic compounds in meteorites, Surv. Geophys. 23 (2002) 411–467, https://doi.org/10.1023/A:1020139302770.
[6] H.-J. Kim, A. Ricardo, H.I. Illangkoon, M.J. Kim, M.A. Carrigan, F. Frye, S.A. Benner, Synthesis of carbohydrates in mineral-guided prebiotic cycles, J. Am. Chem. Soc. 133 (2011) 9457–9468, https://doi.org/10.1021/ja201769f.
[7] A.L. Weber, Prebiotic sugar synthesis: hexose and hydroxy acid synthesis from glyceraldehyde catalyzed by iron(III) hydroxide oxide, J. Mol. Evol. 35 (1992) 1–6, https://doi.org/10.1007/BF00160255.
[8] H.J. Cleaves, Prebiotic chemistry: what we know, What We Don't, Evo Edu Outreach 5 (2012) 342–360, https://doi.org/10.1007/s12052-012-0443-9.
[9] S.L. Miller, H.J. Cleaves, Prebiotic chemistry on the primitive earth, in: I. Rigoutsos, G. Stephanopoulos (Eds.), Systems Biology, Oxford University PressNew, York, NY, 2006, pp. 3–56, https://doi.org/10.1093/oso/9780195300819.003.0001.
[10] J.B. Reece, N.A. Campbell (Eds.), Biology, 9, student ed, Cummings, Boston, Mass. Munich, 2011.
[11] M. Elsafi, Y. Koraim, M. Almurayshid, F.I. Almasoud, M.I. Sayyed, I.H. Saleh, Investigation of photon radiation attenuation capability of different clay materials, Materials 14 (2021) 6702, https://doi.org/10.3390/ma14216702.
[12] A. Negron-Mendoza, S. Ramos-Bernal, The role of clays in the origin of life, in: J. Seckbach (Ed.), Origins, Springer Netherlands, Dordrecht, 2004, pp. 181–194, https://doi.org/10.1007/1-4020-2522-X_12.
[13] R.M. Hazen, D.A. Sverjensky, D. Azzolini, D.L. Bish, S.C. Elmore, L. Hinnov, R.E. Milliken, Clay mineral evolution, Am. Mineral. 98 (2013) 2007–2029, https://doi.org/10.2138/am.2013.4425.
[14] M.A. Pasek, Rethinking early Earth phosphorus geochemistry, Proc. Natl. Acad. Sci. U.S.A. 105 (2008) 853–858, https://doi.org/10.1073/pnas.0708205105.
[15] M.A. Pasek, M. Gull, B. Herschy, Phosphorylation on the early earth, Chem. Geol. 475 (2017) 149–170, https://doi.org/10.1016/j.chemgeo.2017.11.008.
[16] J.D. Toner, D.C. Catling, A carbonate-rich lake solution to the phosphate problem of the origin of life, Proc. Natl. Acad. Sci. U.S.A. 117 (2020) 883–888, https://doi.org/10.1073/pnas.1916109117.
[17] G. Nichols, Sedimentology and Stratigraphy, second ed., Wiley-Blackwell, Chichester, UK ; Hoboken, NJ, 2009.
[18] B. Chako Tchamabé, G. Carrasco-Núñez, D.P. Miggins, K. Németh, Late pleistocene to holocene activity of Alchichica maar volcano, eastern trans-Mexican volcanic belt, J. S. Am. Earth Sci. 97 (2020) 102404, https://doi.org/10.1016/j.jsames.2019.102404.
[19] G. Vilaclara, M. Chávez, A. Lugo, H. González, M. Gaytán, Comparative description of crater-lakes basic chemistry in Puebla State, Mexico, SIL Proceedings, 1922-2010 25 (1993) 435–440, https://doi.org/10.1080/03680770.1992.11900158.
[20] J. Kaźmierczak, S. Kempe, B. Kremer, P. López-García, D. Moreira, R. Tavera, Hydrochemistry and microbialites of the alkaline crater lake Alchichica, Mexico, Facies 57 (2011) 543–570, https://doi.org/10.1007/s10347-010-0255-8.
[21] M. Caballero, G. Vilaclara, A. Rodríguez, D. Juárez, Short-term climatic change in lake sediments from lake Alchichica, Oriental, Mexico, Geo Int. 42 (2003) 529–537, https://doi.org/10.22201/igeof.00167169p.2003.42.3.942.
[22] M.J. Van Kranendonk, Two types of Archean continental crust: plume and plate tectonics on early Earth, Am. J. Sci. 310 (2010) 1187–1209, https://doi.org/10.2475/10.2010.01.
[23] K. Zahnle, L. Schaefer, B. Fegley, Earth's earliest atmospheres, Cold Spring Harbor Perspect. Biol. 2 (2010), https://doi.org/10.1101/cshperspect.a004895 a004895–a004895.
[24] S. Castillo-Rojas, J.C. Landeros, A. Negrón-Mendoza, R. Navarro-González, Radiolysis of aqueous formaldehyde relevant to cometary environments, Adv. Space Res. 12 (1992) 57–62, https://doi.org/10.1016/0273-1177(92)90154-P.
[25] F. Orozco D, Análisis Químico Cuantitativo, 20a ed, Porrúa, México, 1994.
[26] J.C. Westwall, J.L. Zachary, F.M.M. Morel, MINEQL, A Computer Program for the Calculation of Chemical Equilibrium Composition of Aqueous Systems, Tech Note 18, Dept. Of Civil Eng, Mass. Inst. Technol., Cambridge, MA, 1976.
[27] D.S. Brown, J.D. Allison, MINTEQA1, an Equilibrium Metal Speciation Model: User's Manual, U.S. Environmental Protection Agency, Athens, GA, 1987. EPA/600/3-87/012.
[28] W.M. White, Geochemistry, John Wiley & Sons Inc, Hoboken, NJ, 2013.
[29] G. Feulner, The faint young Sun problem, Rev. Geophys. 50 (2012) 2011RG000375, https://doi.org/10.1029/2011RG000375.
[30] J. Madejová, W.P. Gates, S. Petit, IR spectra of clay minerals, in: Developments in Clay Science, Elsevier, 2017, pp. 107–149, https://doi.org/10.1016/B978-0-08-100355-8.00005-9.
[31] R. Olsson, R. Giesler, J.S. Loring, P. Persson, Adsorption, desorption, and surface-promoted hydrolysis of glucose-1-phosphate in aqueous goethite (α-FeOOH) suspensions, Langmuir 26 (2010) 18760–18770, https://doi.org/10.1021/la1026152.
[32] L. Passauer, H. Bender, S. Fischer, Synthesis and characterisation of starch phosphates, Carbohydrate Polymers 82 (2010) 809–814, https://doi.org/10.1016/j.carbpol.2010.05.050.
[33] Y. Tang, F. Cheng, Z. Feng, G. Jia, C. Li, Stereostructural elucidation of glucose phosphorylation by Raman optical activity, J. Phys. Chem. B 123 (2019) 7794–7800, https://doi.org/10.1021/acs.jpcb.9b05968.
[34] H.J. Cleaves Ii, The prebiotic geochemistry of formaldehyde, Precambrian Res. 164 (2008) 111–118, https://doi.org/10.1016/j.precamres.2008.04.002.
[35] A. López-Islas, M. Colín-García, A. Negrón-Mendoza, Stability of aqueous formaldehyde under γ irradiation: prebiotic relevance, Int. J. Astrobiol. 18 (2019) 420–425, https://doi.org/10.1017/S1473550418000368.
[36] S.A. Benner, H.-J. Kim, E. Biondi, Prebiotic chemistry that could not not have happened, Life 9 (2019) 84, https://doi.org/10.3390/life9040084.
[37] S. Haas, K.P. Sinclair, D.C. Catling, Biogeochemical explanations for the world's most phosphate-rich lake, an origin-of-life analog, Commun Earth Environ 5 (2024) 28, https://doi.org/10.1038/s43247-023-01192-8.
[38] L.W.A. Hardie, H.P. Eugster, The evolution of closed-basin brines, Mineral Society of America 3 (1970) 273–290.
[39] D. McConnell, Apatite: its Crystal Chemistry, Mineralogy, Utilization, and Geologic and Biologic Occurrences, Springer Vienna, Vienna, 1973.
[40] I.M. Power, P.A. Kenward, G.M. Dipple, M. Raudsepp, Room temperature magnesite precipitation, Cryst. Growth Des. 17 (2017) 5652–5659, https://doi.org/10.1021/acs.cgd.7b00311.
[41] T. Rinder, M. Dietzel, A. Leis, Calcium carbonate scaling under alkaline conditions – case studies and hydrochemical modelling, Appl. Geochem. 35 (2013) 132–141, https://doi.org/10.1016/j.apgeochem.2013.03.019.
[42] C.A. Fuentes-Carreón, J.A. Cruz-Castañeda, E. Mateo-Martí, A. Negrón-Mendoza, Stability of DL-glyceraldehyde under simulated hydrothermal conditions: synthesis of sugar-like compounds in an iron(III)-Oxide-Hydroxide-Rich environment under acidic conditions, Life 12 (2022) 1818, https://doi.org/10.3390/life12111818.

[43] I.V. Delidovich, A.N. Simonov, O.P. Pestunova, V.N. Parmon, Catalytic condensation of glycolaldehyde and glyceraldehyde with formaldehyde in neutral and weakly alkaline aqueous media: kinetics and mechanism, Kinet. Catal. 50 (2009) 297–303, https://doi.org/10.1134/S0023158409020219.
[44] A.R. Mermut, Baseline studies of the clay minerals society source clays: chemical analyses of major elements, Clay Clay Miner. 49 (2001) 381–386, https://doi.org/10.1346/CCMN.2001.0490504.
[45] S. Söderholm, Y.H. Roos, N. Meinander, M. Hotokka, Raman spectra of fructose and glucose in the amorphous and crystalline states, J Raman Spectroscopy 30 (1999) 1009–1018, https://doi.org/10.1002/(SICI)1097-4555(199911)30:11<1009::AID-JRS436>3.0.CO;2.
[46] C. Godinot, M. Gaysinski, O.P. Thomas, C. Ferrier-Pagès, R. Grover, On the use of ^{31}P NMR for the quantification of hydrosoluble phosphorus-containing compounds in coral host tissues and cultured zooxanthellae, Sci. Rep. 6 (2016) 21760, https://doi.org/10.1038/srep21760.
[47] M. Badertscher, P. Bühlmann, E. Pretsch, Structure Determination of Organic Compounds: Tables of Spectral Data, fourth ed., Springer Berlin Heidelberg, Berlin, Heidelberg, 2009 https://doi.org/10.1007/978-3-540-93810-1.
[48] L.L. Clark, E.D. Ingall, R. Benner, Marine organic phosphorus cycling; novel insights from nuclear magnetic resonance, Am. J. Sci. 299 (1999) 724–737, https://doi.org/10.2475/ajs.299.7-9.724.
[49] D.G. Gorenstein, B.A. Luxon, ^{31}P NMR, in: Encyclopedia of Spectroscopy and Spectrometry, Elsevier, 1999, pp. 2204–2212, https://doi.org/10.1016/B978-0-12-374413-5.00242-6.
[50] V.F. Taylor, R.E. March, H.P. Longerich, C.J. Stadey, A mass spectrometric study of glucose, sucrose, and fructose using an inductively coupled plasma and electrospray ionization, Int. J. Mass Spectrom. 243 (2005) 71–84, https://doi.org/10.1016/j.ijms.2005.01.001.
[51] W. Chai, V. Piskarev, A.M. Lawson, Negative-ion electrospray mass spectrometry of neutral underivatized oligosaccharides, Anal. Chem. 73 (2001) 651–657, https://doi.org/10.1021/ac0010126.
[52] X. Shen, H. Perreault, Characterization of carbohydrates using a combination of derivatization, high-performance liquid chromatography and mass spectrometry, J. Chromatogr. A 811 (1998) 47–59, https://doi.org/10.1016/S0021-9673(98)00238-6.
[53] Z. El Rassi (Ed.), Carbohydrate Analysis: High Performance Liquid Chromatography and Capillary Electrophoresis, Elsevier, Amsterdam ; New York, 1995.
[54] J. McMurry, Organic Chemistry, 8e ed., Brooks/Cole, Cengage Learning, Belmont, CA, 2012.
[55] A. Omran, C. Menor-Salvan, G. Springsteen, M. Pasek, The messy alkaline formose reaction and its link to metabolism, Life 10 (2020) 125, https://doi.org/10.3390/life10080125.
[56] B.W. Darvell, More chemistry, in: Materials Science for Dentistry, Elsevier, 2018, pp. 771–789, https://doi.org/10.1016/B978-0-08-101035-8.50030-4.
[57] G. Wächtershäuser, Pyrite Formation, the first energy source for life: a hypothesis, Syst. Appl. Microbiol. 10 (1988) 207–210, https://doi.org/10.1016/S0723-2020(88)80001-8.
[58] M.J. Russell, A.J. Hall, The emergence of life from iron monosulphide bubbles at a submarine hydrothermal redox and pH front, JGS 154 (1997) 377–402, https://doi.org/10.1144/gsjgs.154.3.0377.
[59] C.S. Chen, Water activity – concentration models for solutions of sugars, salts and acids, J. Food Sci. 54 (1989) 1318–1321, https://doi.org/10.1111/j.1365-2621.1989.tb05982.x.
[60] A. Dinane, M.E. Guendouzi, A. Mounir, Hygrometric determination of water activities, osmotic and activity coefficients of (NaCl+ KCl)(aq) at T= 298.15 K, J. Chem. Therm. 34 (2002) 423–441, https://doi.org/10.1006/jcht.2001.0845.
[61] J. Mazurkiewicz, P. Tomasik, J. Zapłotny, Relationships between water activity and viscosity of solutions, Food Hydrocolloids 15 (2001) 43–46, https://doi.org/10.1016/S0268-005X(00)00048-5.